MRI Relaxation Rates: A Quantitative Approach to Track Tumour Cells Expressing MagA

Anindita Sengupta, *The University of Western Ontario*

Supervisor: Dr. Neil Gelman, *The University of Western Ontario*
Joint Supervisor: Dr. Donna Goldhawk, *The University of Western Ontario*
A thesis submitted in partial fulfillment of the requirements for the Master of Science degree in Medical Biophysics
© Anindita Sengupta 2014

MRI RELAXATION RATES: A QUANTITATIVE APPROACH TO TRACK TUMOUR CELLS EXPRESSING MAGA

(Thesis format: Monograph)

by

Anindita <u>Sengupta</u>

Graduate Program in Medical Biophysics
Collaborative Graduate Program in Molecular Imaging

A thesis submitted in partial fulfillment
of the requirements for the degree of

Master of Science

The School of Graduate and Postdoctoral Studies

Western University
London, Ontario, Canada

July 2014

ABSTRACT

Using magnetic resonance imaging, relaxation rate measurements were performed in cancer cells overexpressing a magnetotactic bacterial gene, MagA. Measurements of magnetic resonance relaxation rates in this expression system is important for optimizing cell detection and specificity, for developing quantification methods, and for refinement of gene-based iron contrast using magnetosome associated genes. We measured the total transverse relaxation rate ($R2^*$), its irreversible and reversible components ($R2$ and $R2'$, respectively) and the longitudinal relaxation rate ($R1$) in MDA-MB-435 tumor cells. Clonal lines overexpressing MagA were cultured in the presence and absence of iron supplementation, and mounted in a spherical phantom for relaxation rate measurements at 3Tesla. In addition to MR measures, cellular changes in iron were evaluated by inductively-coupled plasma mass spectrometry. Values of $R2^*$ and $R2'$ were significantly higher ($p < .01$, accounting for multiple comparisons) in iron-supplemented, MagA- expressing cells compared to unsupplemented cells. $R2^*$ provided the greatest absolute difference and $R2'$ showed the greatest relative difference, consistent with the notion that $R2'$ may be a more specific indicator of iron-based contrast than $R2$, as has been observed in brain tissue. $R2$ differences

between the supplemented and non-supplement MagA-expressing cells showed a trend

($p < .05$) toward significance. R1 differences between these conditions were not significant.

For parental cells, no significant differences between iron-supplemented and unsupplemented

cells were observed in any of the relaxation rates. The results highlight the potential of

magnetotactic bacterial gene expression for detecting labeled cells.

Keywords: Magnetic resonance imaging, MagA, relaxation rates, iron, cancer cells

ACKNOWLEDGMENTS

Besides, I would like to thank Wendy Hough and Dr. Hanif Ladak for supporting and

helping me out in every possible way they could so that I can finish my graduation in time

with ease when I had to face hard times in my life : both joy and sorrow at their extremities.

My graduation would not have been possible without their help.

To my lab members Karina Quiaoit and Linshan Liu, I am grateful and

owe many thanks for all their help and involvement both in lab and in my personal life.

Thanks for staying back with me late nights, in the lab, during my advanced pregnancy

period. I cannot say thanks enough to what you have both done to me.

Thanks to my office mates, Reggie Taylor and Harini Pandithasekera for all their

encouragements and help.

Last, but not the least, I thank my family: My parents, Tapan and Gayatri Sengupta,

for giving me life in the first place, for educating me and for unconditional support and

encouragement to pursue my interests; My husband, Subhasish whose love and support made

me to achieve my goal even after my marriage and especially my little, one year old, bundle

of joy, My daughter, Prisha who gave me the courage and strength to overcome all the

hurdles that came to my life, including the unexpected loss of my dad. Thanks to my in-laws

for their support. Above all, thanks to Almighty God

TABLE OF CONTENTS

CHAPTER 1: INTRODUCTION

CHAPTER 2: RELAXATION RATE MEASUREMENTS IN MAGA-EXPRESSING CANCER CELLS

CHAPTER 3: SUMMARY AND FUTURE WORK

LIST OF TABLES

LIST OF FIGURES

LIST OF ABBREVIATIONS

μ	magnetic moment
γ	gyromagnetic ratio
ω_0	larmor frequency
2D	two-dimensional
ANOVA	analysis of variance
B0	static magnetic field
B1	radio frequency magnetic field
BCA	bicinchoninic acid assay
CPMG	Carr-Purcell-Meiboom-Gill sequence
CT	X-ray computed tomography
FID	free induction decay
GE	gradient echo
ICP-MS	inductively-coupled plasma mass spectrometry
M	magnetization
MR	magnetic resonance
MRI	magnetic resonance imaging
MRS	magnetic resonance spectroscopy
NMR	nuclear magnetic resonance
PBS	phosphate buffered saline
PET	positron emission tomography
RF	radio frequency
SD	standard deviation
SE	spin echo
SEM	standard error of mean
SPECT	single photon emission computed tomography
SPIO	superparamagnetic iron oxide
R1	longitudinal relaxation rate

R2*	transverse relaxation rate
R2	irreversible component of transverse relaxation rate
R2$^{'}$	reversible component of transverse relaxation rate
RIPA	radioimmunoprecipitation assay buffer
ROI	region of interest
T	Tesla
T1	longitudinal relaxation time
T2*	transverse relaxation time
T2	irreversible component of transverse relaxation time
T2$^{'}$	reversible component of transverse relaxation time
TE	echo time
TR	repetition time
TI	inversion time
US	ultrasound
x	x Cartesian coordinate
y	y Cartesian coordinate
z	z Cartesian coordinate

Chapter 1

1.1   Molecular Imaging and Image-Based Cell Tracking

The further development of molecular imaging techniques, involving the

improvement and testing of unique tools and reagents as a means to detect molecular

pathways in vivo, is a current area of research which is growing rapidly [1-4]. This type of

imaging provides a non-invasive way of monitoring processes leading to disease, from

diagnosis through therapy. Molecular imaging can potentially enable one to monitor cellular

activity in terms of location, distribution and long term viability. Scientific accomplishments

have been obtained through various imaging systems, such as bioluminescence and

fluoresecence, computed tomography (CT), positron emission tomography (PET), single

photon emission computed tomography (SPECT), ultrasonography (US), magnetic resonance

spectroscopy (MRS) and magnetic resonance imaging (MRI). Each of these imaging

modalities has its own advantages and disadvantages.

Of the various imaging platforms, MRI, has distinguished itself as a promising

system. The strengths of MRI, the imaging modality used in this thesis, include the ability to

image at any tissue depth [5] and to provide excellent soft tissue contrast with high spatial

resolution [6]. Since its introduction over 25 years ago, MRI has been applied to longitudinal

studies [7, 8] and the repetitive monitoring of processes like therapeutic stem cell

engraftment, cancer growth and metastasis, changes in pancreatic beta cell function during

diabetes and cardiac cell activity after heart attack [9]. In spite of these strengths, MRI fails

to track cellular and molecular activities as has been achieved in optical imaging using

reporter genes such as the green fluorescent protein and luciferase [2, 10]. While these

reporters may provide fine spatial and temporal information for cell microscopy, in vivo

optical imaging of live animals is limited to superficial regions because of the absorption and

scattering of light. Of the non-invasive in vivo imaging modalities, MRI has relatively high

spatial resolution and allows long-term repetitive imaging, without using ionizing radiation.

However, MRI fails to show high sensitivity compared to SPECT and bioluminescence

imaging. In order to take advantage of MRI in image-based cell tracking, labeling of cells is

required to improve bio-imaging at the cellular and molecular level [11].

1.2   Cell Tracking using MRI

Progressive molecular imaging techniques cater to advanced and improved ways for

quantitative cell tracking. In order to detect transplanted cells using MRI, cells need to be

labeled with magnetic contrast agents. Initially most methods for tracking cells

involved the use of exogenous labels, such as superparamagnetic iron oxide (SPIO)

nanoparticles because of the high sensitivity of detecting these labeled cells [12, 13]. This

high sensitivity is due to the large amount of SPIO iron that can be taken up. For example,

single cell MRI detection has been accomplished in one study where the average iron content

per cell was approximately 70 pg [14]. Gene based methods have also been under

development to address one of the problems with SPIO nanoparticle labeling: dilution of the

particle following repeated cell divisions. Another shortcoming of SPIO particles concerns

their localization upon cell death. For example, macrophages engulf dead cells and may

release the iron in a spatially and temporally different pattern than the original host cell. As a

result of this, the free SPIO may remain in the body and show MR contrast which can be

misleading [15]. In a report by Amsalem et al. it was shown that MRI signal voids were not

from the SPIO labeled transplanted cells but instead from the cardiac macrophages which

took up the free SPIO [16]. Haacke et al. also showed that free SPIO released by dead cells

was taken up either by macrophages or nested in the local tissue [17]. To effectively monitor

cell location and activity it is essential to be able to specifically detect live cells. Various

methods of overcoming the limitations of cell tracking with exogenous cell labeling have

3

been adapted including the use of endogenous or gene-based labels.

1.3   MRI using Gene-Based Label

To circumvent the problems associated with cell tracking using SPIO nanoparticles,

described above, genetic engineering methods have been employed to overexpress genes

involved in the transport and storage of iron thereby leading to an increase in the intracellular

level of iron [9]. Various methods and proteins dealing with iron have been studied for their

proficiency as MR contrast agents, along with those recognized for their primary function in

mammalian iron homeostasis: iron response elements [18], transferrin receptor [19] and

ferritin subunits [20]. Part of the challenge in adapting iron binding proteins for use in

generating MR contrast relates to the elaborate control of iron homeostasis in mammalian

cells [21] and the manner in which this may fluctuate in response to changes in physiological

state [22]. The development of these gene-based contrast agents for MRI leads to the

possibility of imaging reporter gene expression and pathology in transgenic animals [23].

Although the evolution of gene-based, MR contrast for cell tracking and the MRI

methodology used for its detection is progressing it requires further development.

Research in the last decade has revealed that iron biomineral formation is a

phenomenon that can occur naturally in the animal kingdom. Magnetotactic bacteria are an extraordinary example of how single cells may synthesize and compartmentalize an iron biomineral, magnetite (Fe_3O_4), in a membrane-enclosed magnetosome [24-26] and harness its magnetic properties [27]. Although an understanding of the molecular nature of the magnetosome is not yet complete, many applications making use of its effect on the MRI signal have been carried out [28, 29]. A more complete understanding of which genes are essential for the synthesis of the basic magnetosome compartment and for the manipulation of select magnetosome features, would permit the versatile use of this structure in the generation of MR contrast for pre/clinical imaging [9].

Several genes involved in the formation of magnetosome and magnetotactic bacteria have been studied. Among these genes, MagA, was one of the first to be identified and has been partially characterized as an iron transport protein [30]. MagA, an integral membrane protein, is potentially involved in the active transport of the large quantity of iron required to support magnetosome formation [31]. As expected, MagA-expression results in iron accumulation in the cell [32]. As a result, this leads to a change in contrast detectable by MRI [33, 34]. Additionally, the estimated iron per cell using this gene-based contrast is close to 0.6 pg/cell [34] and is approximately 100 x lower than the SPIO values provided earlier [14].

There are some advantages and disadvantages of using cells manipulated to overexpress MagA. These advantages are (i) Longitudinal imaging over time can be performed – ideally no dilution of the label occurs with cell division if it is assumed that iron levels in extracellular fluid are sufficiently high. Keeping these iron levels high enough may require iron supplementation of drinking water for animals. (ii) Working with MagA may lead to the development of a reporter gene, i.e., a gene construct capable of monitoring transcription factor activity. Disadvantages of MagA (or other gene-based iron labeling) include the lower sensitivity due to lower iron uptake (approximately 100 times lower compared to SPIO particles) and the complexity of cell preparation.

Recently, contrast due to overexpression of either MagA or the modified ferritin subunits (heavy and light chain, HF + LF), lacking iron response elements to enable continuous expression, were compared in a model of tumour growth from transplanted cells [35]. These studies suggest that magnetotactic bacterial genes, including magnetosome genes, may be effectively used in the future for reporter gene expression for molecular MRI.

1.4   Role of MagA in MRI

Cells with iron-based contrast agents are difficult to differentiate from anatomical features represented as dark regions on MRI because hypointense signals are

6

generated when these contrast agents are used [36]. In this scenario, MagA overexpression may be particularly useful in tracking breast cancer metastasis in the white matter of brain [37]. Recently, a group characterized the temporal pattern of contrast due to the constitutive expression of MagA [35] to utilize this technique in future for reporter gene expression in tumor xenografts.

Previous measurements of MRI relaxation times in MagA-expressing mammalian cells have been carried out. Manipulation of T2 relaxation time (refer to section 1.5.2) for cell detection was assessed in 293FT cells using doxycycline induced expression of MagA, cloned from M. magnetotacticum strain MS-1[33]. The effect of varying concentrations of iron supplement on T2 relaxation rate was examined on a 3T MR scanner using a Carr-Purcell-Meiboom-Gill (CPMG) sequence. The relaxation rate of MagA-expressing cells showed that the measurement of R2 (1/T2) depended on the concentration of iron (ferric nitrate) in the culture medium. In this study by Zurkiya et al., they showed that induction of MagA-expression (by doxycycline) was coordinated with the increase in R2. This not only shows that a molecular interaction can stimulate changes in R2 through a genetic mechanism but also provides strong support for the application of gene-based iron contrast. In this cell line expressing MagA, values of R2 varied roughly between 6-9 s^{-1}.

In 2011, another magnetotactic bacterial gene, Mms6, was reviewed as an MRI

reporter [38]. This small protein associated with Mms6 gene, acidic in nature and showing

high affinity for iron ions [39], was used in 293T cells for investigating the same R2

relaxation rates [40]. The response pattern of the R2 relaxation rate to the iron-supplemented

Mms6-expressing cells was similar to that of the MagA-expressing cells, but R2 was lower in

value (4-6 s^{-1}) in the identical cell line. Although Mms6 has a potential as a reporter gene,

further work is required to demonstrate its efficiency in producing MR contrast.

In another assessment of MR intracellular contrast, MagA cloned from strain AMB-1

was compared to a mutated form [33]. Mouse neuroblastoma (N2A) cells were transfected

with MagA, mutant or vector DNA, cultured in the presence of 250 μM ferric nitrate and

immobilized in gelatin phantoms for imaging at 11T. Based on the image analysis the authors

reported that MagA-expressing cells can produce signal contrast over mutant or vector

controls detectable by MRI. In this same report, the potential of MagA- expressing cancer

cells to grow and generate intracellular contrast in vivo was evaluated on a 3T MRI system.

Human MDA-MB-435 cells were transfected with MagA and transplanted subcutaneously

into the hind limb of immune-deficient mice. The results of this imaging study not only

revealed that tumours formed from MagA-expressing cells generated hypointense signal

regions compared to the parental control but also showed that MagA-expression maintained the biological programming of cancer cells.

Recently, it has also been shown that MR contrast can be observed when the overexpression of MagA from AMB-1was compared to that of modified, mammalian ferritin subunits [35]. In a mouse model of tumor growth, transplanted cells were imaged over 5 weeks in a repetitive manner and compared to the parental cell xenograft. Both MagA- and HF+LF-expressing tumors provided contrast enhancement. Moreover, MagA-derived contrast exhibited greater contrast to noise ratio than HF+LF-expressing tumors, particularly in the immediate days post-injection, indicating a role for select magnetotactic bacterial genes in preclinical molecular imaging.

Despite the fact that very little is recognized regarding the handling of MagA activity in mammalian cells and whether or not MagA activity can be coordinated with precise location of its contrast signal, quantitative measures of iron contrast, such as relaxation rates (see section 1.6), can be of great value in localizing iron-loaded cells in the developing tumor. Relaxation rates provide an objective means for quantifying our observations. Also, such measures may in the future be utilized in developing methods for estimating the number of cells in each voxel.

Before discussing the specific MRI measures used in this thesis, some of the basic principles of MRI will be briefly presented. Since MRI involves creating images of nuclear magnetic resonance (NMR) signals, MRI will be discussed after describing the basics of NMR.

1.5 Nuclear Magnetic Resonance

1.5.1 Basics of NMR

The nature of NMR is based on the interactions of nuclear spins with an external magnetic field. In the classical view, protons are spinning charged particles producing a small magnetic moment [41]. They possess spin, a fundamental property of nature. Protons are fermions or spin ½ particles. They have spin angular momentum, $\vec{S}$, which is associated with a magnetic diploe moment, $\vec{\mu}$ that is oriented along the spin axis and expressed as

$$\vec{\mu} = \gamma \, \vec{S} \qquad\qquad (1.1)$$

where γ, known as the gyromagnetic ratio, is a nuclei specific constant. For protons $(\gamma/2\pi) = 42.576 \times 10^6$ Hertz per Tesla (Hz/T) [41].

Magnetic Moment Direction
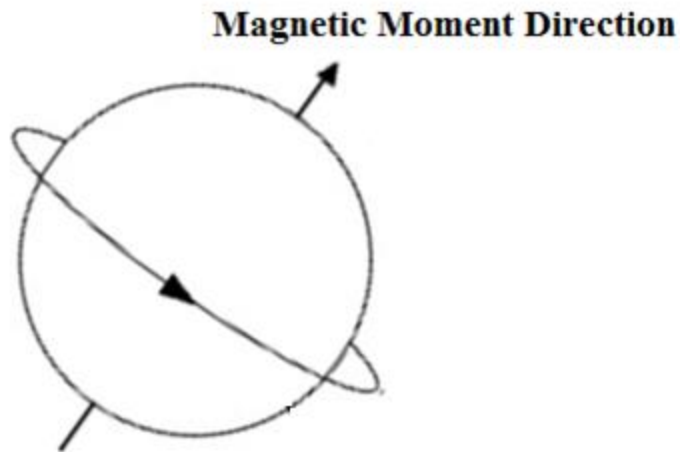
Figure 1.1. Proton spin and its relation to magnetic moment

Magnetic resonance imaging is based on detecting NMR signals from hydrogen

nuclei (single proton), which are the most abundant nuclei present in the body [41]. In

particular it is hydrogen in water (or fat) that gives rise to most of these signals.

The sum of all nuclear magnetic moments in a given volume is known as the nuclear

magnetization ($\vec{M}$). In the context of MRI, $\vec{M}$ usually refers specifically to the nuclear

magnetization from protons in water (or fat). (Signals from hydrogen nuclei in

macromolecules, cell membranes etc. typically decay away too quickly to observe with

conventional MRI.) In the absence of an external magnetic field, the net magnetization is

zero. This is because all the spins are randomly oriented and as a result their magnetic

moments cancel out. If a large external magnetic field ($\vec{B_0}$) is present, the nuclear

magnetic moments partially align with it. Some of the spins align with their z-component

parallel to $\vec{B_0}$ while others align antiparallel to $\vec{B_0}$. However, there are slightly more spins

aligned parallel than antiparallel (difference on the order of 1 in 10^6) to the direction of B_0

giving rise to the net magnetization (M) along this direction (z-direction).

In the classical picture, the spins' magnetic moments precess (clockwise) around the

direction of the external magnetic field at a frequency ω_0 , known as the resonance or

Larmor frequency, determined by

$$\omega_0 \; = \; \gamma \, B_0 \tag{1.2}$$

Since the x, y components of these magnetic moments cancel, the total magnetization,

$\vec{M_0}$ is in the direction of $\vec{B_0}$, [42]. This is known as the "equilibrium state" of the

magnetization (Figure 1.2).
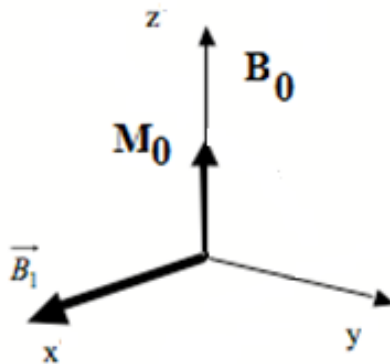
Figure 1.2. Magnetization in equilibrium state. $\vec{M_0}$ is parallel to the external magnetic field $\vec{B_0}$ and is in equilibrium along the field

In order to produce an NMR signal the magnetization must be forced away from

equilibrium. In the classical description when a torque is applied to the magnetization M_0, it

tips away from its initial position (Figure 1.3), parallel to the axis of B_0 or z-axis. This

rotation is accomplished using a time-dependent magnetic field known as a radiofrequency

pulse (RF pulse), B_1.
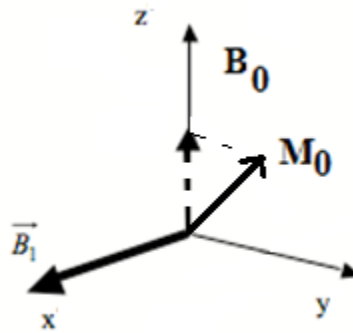
Figure 1.3. Magnetization in a non-equilibrium state. $\overrightarrow{M_0}$ is tipped away from the z-axis
by an RF pulse

The tilted magnetization can be decomposed into two orthogonal components: a

longitudinal or Z component and a transverse component on the XY plane (Figure 1.4).
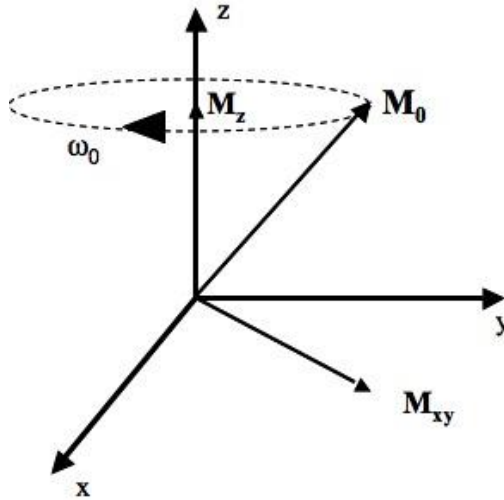
Figure 1.4. Orthogonal components of the magnetization vector

Radiofrequency (RF) pulses create a time-varying magnetic field $\overrightarrow{B_1}$, perpendicular

to $\overrightarrow{B_0}$, oscillating at the Larmor frequency (or close to it). RF pulses can rotate the

magnetization through any angle. In the case of a 90° RF pulse, the net magnetization is

rotated into the *x*, *y* plane. As the magnetization is tipped away from the *z*-axis it begins to

rotate about this axis at the Larmor frequency and this continues following the pulse. The

rotating magnetization (magnetic field) induces a voltage signal in a nearby radiofrequency

coil (antenna).

As soon as the RF pulse ceases, the system or the excited proton spins return from the

unstable state to an equilibrium state. This return of the magnetization to its equilibrium

position is termed "Relaxation". There are two components to relaxation: the decay of M_{xy}

14

and the return of M_z to its equilibrium state.

1.5.2 Transverse Relaxation

The return of M_{xy} to equilibrium or zero value is called transverse relaxation. This

decay is in some cases, an exponential decay process and is characterized by a time constant

known as $T2^*$ or the transverse relaxation time or as a rate $R2^*(1/T2^*)$. This decay is due to

dephasing of the magnetic moments. For example, when a proton spin feels a strong local

magnetic field in the direction of B_0 it will precess faster than average while a proton spin

that feels a local magnetic field in the direction opposite to B_0 will precess slower than

average and these magnetic moments will get out of phase leading to overall signal decay.

There are various sources of transverse magnetization decay including nuclear spin-spin

interactions and local magnetic field variations over distance scales from microscopic to

macroscopic. For example iron particles create spatially non-uniform magnetic fields ranging

over micron or tens of micron distance scales, intermediate between dipolar magnetic fields

(angstroms to nanometers) and the macroscopic magnetic field variations (mm to cm).

During the transverse magnetization decay a second RF pulse that rotates the

magnetization though 180° can be applied and will have the effect of partially reversing the

dephasing described above. Thus there are reversible and irreversible contributions to $R2^*$.

In this thesis we will denote the irreversible and reversible components as $R2$ $(1/T2)$ and $R2'$

$(1/T2')$ respectively, where

$$R2^* = R2 + R2' \hspace{3cm} (1.3)$$

Some authors define $R2$ as being only due to the nuclear spin-spin interactions. However,

other sources of microscopic magnetic field variation, such as that due to iron particles can

lead to partially irreversible transverse magnetization decay due to the effects of water self

diffusion. (Some authors would consider this diffusion effect as an "apparent" contribution to

$R2$.) In particular, a water molecule will likely be in a different location during the

dephasing are rephrasing periods (before and after the $180°$, respectively), and hence, the

dephasing will not be completely rephased. Cellular iron influences both $R2$ and $R2'$ with

the degree of reversibility depending on spatial distribution of particles.

Nuclear spin-spin relaxation is governed by the interactions between proton spins and

their surroundings. In general, each of the proton spins creates a non-uniform local magnetic

field distributed roughly over molecular distance scales. As a result a given nucleus can

experience widely varied local magnetic field values based on the location and orientation of

its neighbours.

In solids, where the local field distribution is almost static, the T2 decay times are on the order of microseconds. In liquids, due to rapid motion of the water molecules, the local magnetic field experienced by each proton changes rapidly thereby reducing effect of the local magnetic fields leading to longer decay times, on the order of milliseconds.

1.5.3. Longitudinal Relaxation

The regrowth of M_z along z-axis takes place through longitudinal or spin-lattice relaxation, characterized by a time constant T1 or the longitudinal relaxation time.

Transitions of excited proton spins to the equilibrium position are due to the local magnetic fields experienced by a single nucleus (1H for water) from its neighbouring nuclei (1H) including neighbor on the same water molecule as well as the nuclei (1H) of nearby water molecules. This local magnetic field fluctuates rapidly because of the rapid motion of the water molecules. The fluctuations are typically spread out over the spectrum from low to very high, much higher than the Larmor frequency (the correlation time for water is roughly on the order of 10^{-12} sec). It is the frequency component at the Larmor frequency that leads to T1 relaxation.

1.5.4. Nuclear Magnetic Resonance Signals

The free induction decay (FID) is the signal obtained following a single RF pulse. The decay of this signal corresponds to the T2* decay of the magnetization described above. The amplitude of this generated signal decays to zero, without losing energy to the environment. In tissues the FID typically has a duration of tens of millisecond.

A spin echo sequence uses a 90° RF pulse followed by a 180° RF pulse. The 90° pulse is applied to tip the total magnetization M_0 into the transverse or XY plane where the spins dephase naturally. Then after a certain time period a 180° pulse is applied in order to partially refocus (only the static part) of the dephased spins. The spins at this point maintain the same precessional frequencies with reversed phase angles. The time period between the 90° and 180° RF pulses is represented by TE/2 which is half of the echo time (TE). After a certain time, equal to the delay between 90° and 180° pulse, the spins partially rephase forming an echo (Figure 1.5).
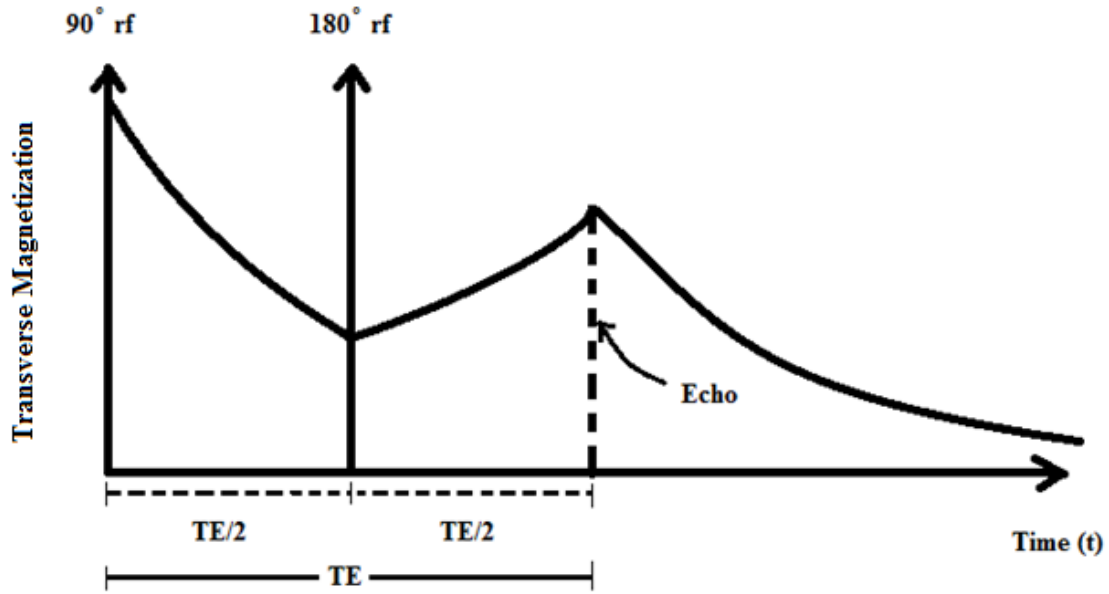
Figure 1.5. Spin echo pulse sequence. 180° RF pulse following a 90° RF pulse refocuses

the spins to create the echo of the signal called the spin echo (SE) at the echo time (TE).

1.6   Magnetic Resonance Imaging (MRI)

Magnetic resonance imaging (MRI) signals are similar to NMR signals but

MRI also involves localization of this signal which is accomplished with magnetic field

gradients. There are three field gradients, one in each of the three directions, x, y and z.

The magnetic field gradient refers to an additional magnetic field that varies linearly in one

of the directions (typically the gradient or slope has a maximum value on the order of tens of

mT/m).

MRI pulse sequences are comprised of RF pulses and gradient magnetic fields.

19

The order, amplitudes, shapes, and spacing of both RF and gradient waveforms are included

in each pulse sequence. Here we will consider conventional spin-echo (SE) and

gradient-echo (GE) pulse sequences as these are relevant to the experiments carried

out for this thesis.

1.6.1 Spin-Echo Imaging

In conventional spin echo imaging (Figure 1.6) the RF pulses are similar to those in

nuclear magnetic resonance (NMR) except that they are slice selective in the case of two-

dimensional (2D) acquisitions. RF pulses combine with a gradient to generate a rotation

angle typically between 0° and 90° for protons that are located within a slice of tissue

(typically a few mm thick). Localization within the plane of the image is accomplished by

frequency encoding in one direction and phase-encoding in the orthogonal direction. The

frequency encoding gradient when applied in one direction creates linear variation of

precession frequencies along that direction which encodes the positions of the resonating

spins based on the frequency of their signals. The phase encoding gradient, is utilized to

impart a specific phase angle to the transverse magnetization. This angle depends on the area

under the phase encoding gradient lobe and the position of the spins along the phase

encoding direction. Phase encoding is accomplished by repeating the signal acquisition (Ny

times, see Figure 1.6) while incrementing the area under the phase encoding lobe each time.

The spatial information is encoded in the phase of the signals. In acquiring a SE image the

segment shown in Figure 1.6 is repeated Ny times, where Ny, is the number of phase

encoding steps (equal to the matrix size of the image in the phase encoding direction). The

time between each of these segments is called the repetition time TR.
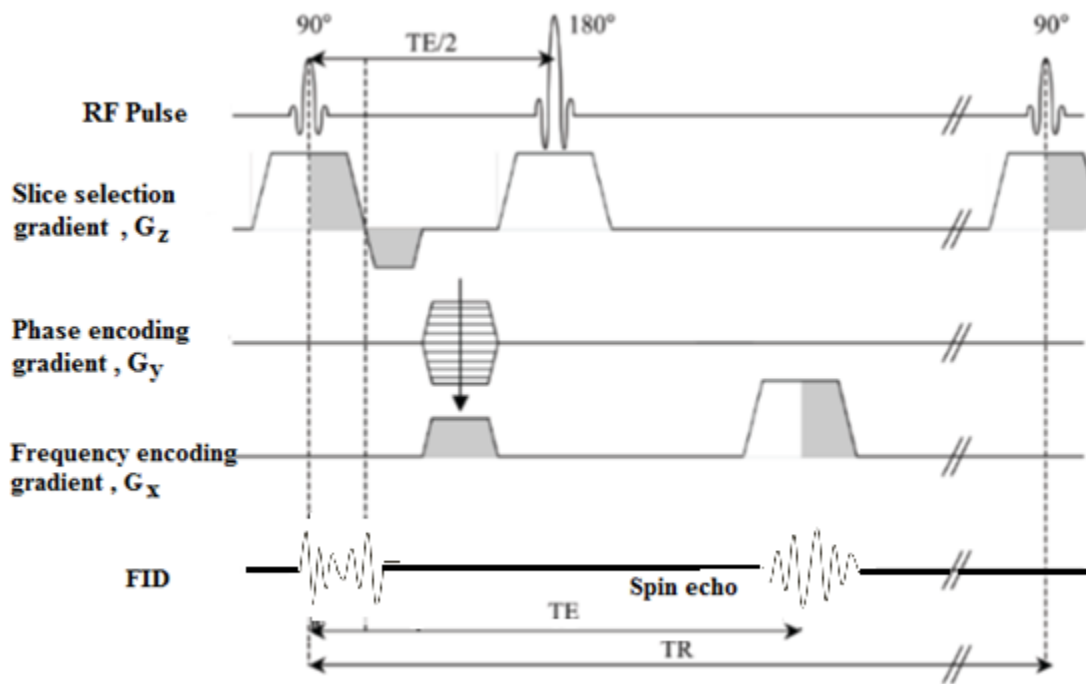
Figure 1.6. Pulse sequence diagram for conventional spin-echo imaging.

The amplitude of a simple spin-echo signal, in the limit where TR >> TE, is given by the

following equation:

$$S\ (TE, TR) \approx kM_0\ \{\ 1 - \exp[-TR/T1]\}\ \exp\ (-TE/T2) \qquad (1.4)$$

However, a closer approximation is given by replacing TR by TR – TE, given by [43]

$$S\ (TE, TR) \approx kM_0\ \{\ 1 - \exp[-(TR - TE)/T1]\}\ \exp\ (-TE/T2) \qquad (1.5)$$

1.6.2 Gradient-Echo Imaging

The GE sequence is simpler than SE sequence and uses a single RF pulse followed by

a gradient pulse to generate the echo. The scan times for GE sequences can be much shorter

than for SE sequences because short TR times can be used if small flip angles are employed

for excitation. In GE sequences, gradient reversal is used to form the gradient echo [45, 46]

instead of the 180° refocusing pulse, used for echo formation in the SE sequence. Gradient

reversal is applied with the frequency encoding gradient and hence this gradient performs the

function of echo formation and spatial encoding along one dimension. The amplitude of the

single gradient-echo signal (Figure 1.7) is similar to the FID signal assumed to be

exponential, given by

$$S\ (TE, TR) \approx kM_0\ [\ 1 - \exp(-TR/T1)]\ \exp\ (-TE/T2^*) \qquad (1.6)$$
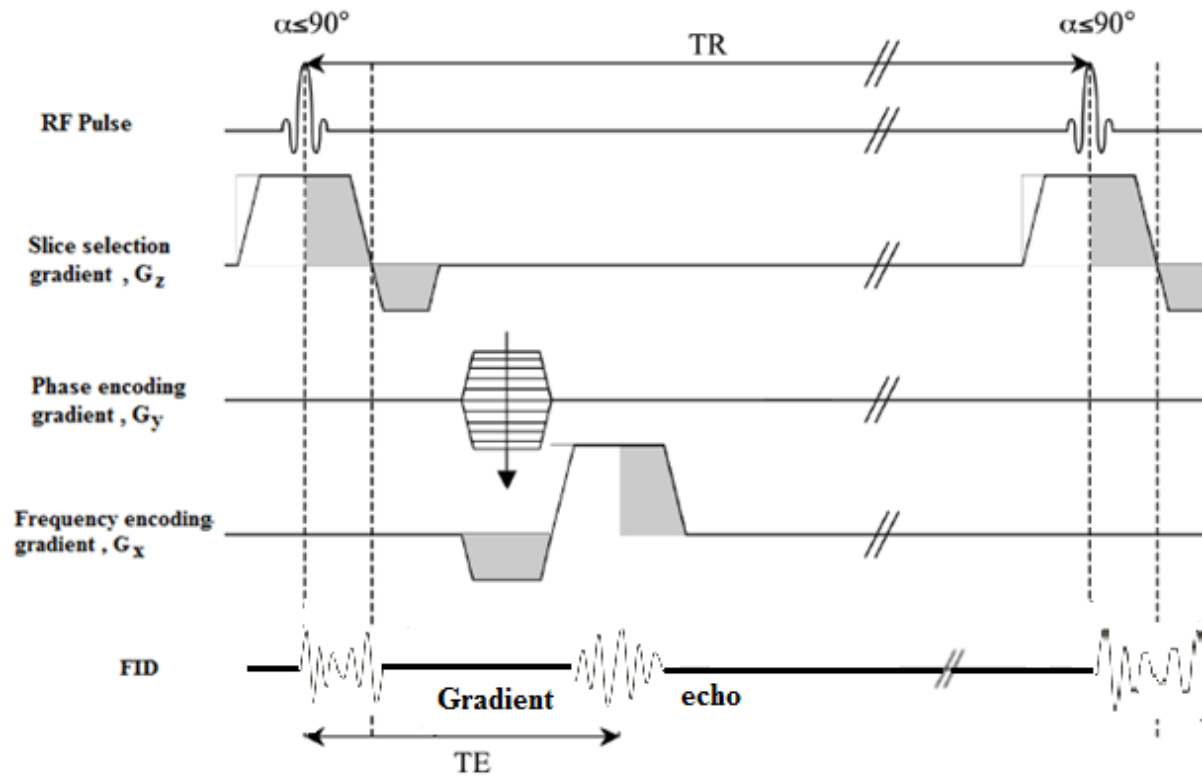
Figure 1.7. Simple single gradient echo pulse sequence. Excitation pulse is followed by a gradient pulse which makes the spins to rephase and form a gradient echo.

The multi-echo gradient echo sequence is similar to the single-echo gradient echo sequence except that in this case signals at multiple TE's are acquired within each TR period.

1.6.3 Inversion Recovery Spin-echo Imaging

The inversion recovery spin-echo sequence, is applied in my thesis for the measurement of R1 (1/T1). The pulse sequence is similar to that of the spin-echo, except that an additional 180° RF pulse is included prior to the 90° RF pulse. This initial 180° pulse

inverts the z-magnetization and hence is referred to as an inversion pulse. The time delay

between the inversion pulse and the 90° pulse is known as the inversion time (TI).

The inversion recovery spin-echo signal is given by

$$S\,(TE) = kM_0\,\{1 - 2\exp-(TI/T1) + \exp\,(-TR/T1)\}\,exp\,(-TE/T2) \qquad (1.7)$$

1.7 Thesis Overview

There is a great deal of interest in developing magnetic resonance imaging (MRI)

methods to monitor the location of cancer cells as well as their molecular activity in animal

models of tumor growth and metastasis. Labeling cancer cells with iron nanoparticles

provides a means of detection and localization. Iron particles create a microscopically non-

uniform magnetic field, which in turn, influences fundamental MRI parameters called

relaxation rates.

The most common method of iron-based cell labeling involves the introduction of

exogenous superparamagnetic iron oxide nanoparticles. Although this provides high

sensitivity for cell detection, the potential for long-term monitoring is limited due to

degradation, dilution of the label during cell division and lack of inherent biological activity.

Alternatively, gene-based contrast imparts endogenous magnetic characteristics to cells, thus,

creating a tracking system suitable for long-term, repetitive imaging of cellular function, including migration, mitosis and differentiation. In mammalian cancer cells, Goldhawk et al. [33] and Zurkiya et al. [34] have previously demonstrated that expression of MagA, a putative iron transport protein from magnetotactic bacteria, leads to observable alterations in the MR signal.

The goal of my work was to quantify the effect of MagA -based iron labeling on MRI relaxation rates in order to provide insight into designing methods in the future for tracking these cells in-vivo. As mentioned earlier, both R2 and $R2^{*}$ are influenced by iron and other tissue properties. However, studies related to $R2^{'}$ measurements in tissues showed that $R2^{'}$ was more characteristic of iron content than R2 [47]. Hence, the work in this thesis also includes assessing $R2^{'}$ as a measure for detecting these labelled cells. My hypothesis is that $R2^{'}$ will provide a stronger indicator to detect iron supplementation in MagA samples and will correlate more strongly with iron content as compared to other relaxation rates. The experiments are carried out using MDA-MB-435 cells, a highly metastatic and aggressive cell line that was genetically engineered to overexpress MagA, in order to generate gene-based contrast.

In Chapter 2, an imaging design, involving quantification of the MRI signal

changes associated with cellular iron uptake by MagA-expressing cells has been applied

to track gene-based iron-labeled cells. This quantification is based on measuring the MRI

relaxation rates ($R2^*$, $R2$, $R2'$ and $R1$) in cultured MagA-expressing cells and in the

untransfected parental cell line (MDA-MB-435), as a control. Using 3 Tesla (T) MRI and

gelatin phantoms, my thesis demonstrates how the relaxation rates vary as a function of iron

supplementation. Results are also examined in light of elemental iron content to reflect the

degree of iron uptake.

In Chapter 3, the findings in chapter 2 are highlighted to address the efficiency of a

single magnetotactic bacterial gene as an MR contrast agent, subject to genetic control. A

summary of the findings along with future directions of this research are also provided.

1.8　REFERENCES

1. Hoffman, J.M. and Gambhir, S.S., *Molecular imaging: the vision and oppurtunity for radiology in the future.* Radiology, 2007. **44**: p. 39-47.

2. Massoud, T.F. and Gambhir, S.S., *Molecular imaging in living subjects: seeing fundamental biological processes in a new light.* Genes Dev, 2003. **17**: p. 545-580.

3. Ye, Y. and Chen, X., *Integrin targeting for tumor optical imaging.* Theranostics, 2011. **1**: p. 102-126.

4. Margolis, D.J., Hoffman, J.M., Herfkens, R.J., Jeffrey, R.B., Quon, A. and Gambhir, S.S., *Molecular imaging techniques in body imaging.* Radiology, 2007. **245**: p. 333-356.

5. Burtea, C., Laurent, S., Vander, Elst L., and Muller, R., *Contrast Agents: Magnetic Resonance* in *Molecular Imaging I.* 2008, Heidelberg: Springer-Verlag Berlin. p. 135-165.

6. Hartung, A., Lisy, M. R.,Herrman, K.-H.,Hilger, I., Schuler, D., Lang, C., Bellemann, M. E., Kaiser, W. A. and Reichenbach, J. R., *Labeling of macrophages using bacterial magnetosomes and their characterization by magnetic resonance imaging.* Magnetism and Magnetic Materials, 2006. **311**: p. 454-459.

7. Bulte, J.W., Duncan, I.D. and Frank, J.A., *In vivo magnetic resonance tracking of magnetically labeled cells after transplantation.* Cereb Blood Flow Metab, 2002. **22(8)**: p. 899-907.

8. Bulte, J.W., *In vivo MRI cell tracking: clinical studies.* AJR Am J Roentgenol 2009. **193 (2)**: p. 314-325.

9. Goldhawk, D., Rohani, R., Sengupta, A., Gelman, N. and Prato F., *Using the magnetosome to model effective gene-based contrast for magnetic resonance imaging.* WIRES Nanomed Nanobiotechnol, 2012. **4**: p. 378-388.

10. Ntziachristos, V., *Going deeper than microscopy : the optical imaging frontier in biology.* Nat Methods, 2010. **7**: p. 603-614.

11. Li, Li., Jiang,Wen., Luo, Kui., Song, Hongmei., Lan, Fang., Wu, Yao. and Gu, Zhongwei., *Superparamagnetic Iron Oxide Nanoparticles as MRI contrast agents for Non-invasive Stem Cell Labeling and Tracking.* Theranostics, 2013. **3(8)**: p. 595-615.

12. Hill, J.M., Dick, A.J., Raman, V.K., Thompson, R.B., Yu, Z.X., Hinds,K.A.,Pessanha, B.S., Guttman, M.A., Varney, T.R., Martin, B.J., Dunbar, C.E., McVeigh, E.R. and Lederman, R.J., *Serial cardiac magnetic resonance imaging of injected mesenchymal stem cells.* Circulation, 2003. **108(8)**: p. 1009-1014.

13. Kraitchman, D.L., Tatsumi, M., Gilson, W.D., Ishimori, T., Kedziorek, D., Walczak, P., Segars, W.P., Chenn, H.H., Fritzges, D., Izbudak, I., Young, R.G., Marcelino,M., Pittenger, M.F., Solaiyappan, M., Boston, R.C., Tsui, B.M., Wahl, R.L. and Bulte, J.W., *Dynamic imaging of allogeneic mesenchymal stem cells trafficking to myocardial infarction.* Circulation, 2005. **112(10)**: p. 1451-1461.

14. Heyn, C., Ronald, J.A., Mackenzie, L.T., MacDonald, I.C., Chambers, A.F., Rutt, B.K., and Foster, P.J., *In vivo magnetic resonance imaging of single cells in mouse brain with optical validation.* Magnetic Resonance in Medicine, 2006. **55**: p. 23-29.

15. Terrovitis, J., Stuber, M., Youssef, A., et al., *Magnetic resonance imaging overestimates ferumoxide-labeled stem cell survival after transplantation in the heart.* Circulation, 2008. **117**: p. 1555-1562.

16. Amsalem,Y., Mardor,Y., Feinberg, M.S., et al., *Iron-oxide labeling and outcome of transplanted mesenchymal stem cells in the infarcted myocardium.* Circulation, 2007. **116**((11 Suppl)): p. 138-145.

17. Haacke, E.M., Cheng, N.Y., House, M.J., Liu, Q., Neelavalli, J., Ogg, R.J., Khan, A., Ayaz, M., Kirsch, W. and Obenaus, A., *Imaging iron stores in the brain using magnetic resonance imaging.* Magn. Reson. Imaging, 2005. **23**: p. 1-25.

18. Genove, G., Demarco, U., Xu, H., Goins, W.F. and Ahrens, E.T., *A new transgene reporter for in vivo magnetic resonance imaging.* Nat. Med., 2005. **11**: p. 450-454.

19. Deans, A.E., Wadghiri, Y.Z., Bernas, L.M., Yu, X., Rutt, B.K. and Turnbull, D.H., *Cellular MRI contrast via coexpression of transferrin receptor and ferritin.* Magn Reson Med, 2006. **56**: p. 51-59.

20. Cohen, B., Ziv, K., Plaks, V., Harmelin, A. and Neeman, M., *Ferritin nanoparticles as magnetic resonance reporter gene.* WIRES Nanomed Nanobiotechnol, 2009. **1**: p. 181-188.

21. Pantopolous, K., Porwal, S., Tartakoff, A. and Devireddy, L. , *Mechanisms of mammalian iron homeostasis.* Biochemistry, 2012. **51**: p. 5705-5724.

22. Recalcati, S., Locati, S., Marini, A., Santambrogio, P., Zaninotto, F., DePizzol, M., Zammataro, L., Girelli, D. and Cairo, G. , *Differential regulation of iron homeostasis during human macrophage polarized activation.* Eur J Immunol, 2010. **40**: p. 824-835.

23. Cohen, B., Ziv, K., Plaks, V., Israely, T., Kalchenko, V., Harmelin, A., Benjamin, L.E. and Neeman, M., M*RI detection of transcriptional regulation of gene expression in transgenic mice. .* Nat Med, 2007. **13(4)**: p. 498-503.

24. Arakaki, A., Nakazawa, H., Nemoto, M., Mori, T. and Matsunaga, T., *Formation of magnetite by bacteria and its application.* J R Soc Interface, 2008. **5**: p. 977-999.

25. Murat, D., Byrne, M. and Komeili, A., *Cell biology of prokaryotic organelles.* Cold Spring Harb Perspect Biol, 2010. **2(10)**: p. a000422.

26. Schuler, D., *Genetics and cell biology of magnetosome formation in magnetotactic bacteria.* FEMS Microbiol Rev, 2008. **32(4)**: p. 654-672.

27. Komeili, A., *Molecular mechanisms of compartmentalization and biomineralization in magnetotactic bacteria.* FEMS Microbiol Rev, 2012. **36**: p. 232-255.

28. Takahasi, M., Yoshino, T., Takeyama, H. and Matsunaga, T., *Direct magnetic separation of immune cells from whole blood using bacterial magnetic particles displaying protein G.* Biotechnol Prog, 2009. **25**: p. 219-226.

29. Yan, L., Zhang, S., Chen, P., Liu, H., Yin, H. and Li, H., *Magnetotactic bacteria, magnetosomes and their application.* Microbiol Res, 2012. **167**: p. 507-519.

30. Nakamura, C., Burgess, J. G., Sode, K. and Matsunaga, T., *An iron-regulated gene, magA, encoding an iron transport protein of Magnetospirillum sp. strain AMB-1.* J Biol Chem, 1995. **270(47)**: p. 28392-28396.

31. Faivre, D. and Schuler, D., *Magnetotactic bacteria and magnetosomes.* Chem Rev, 2008. **108**: p. 4875-4898.

32. Sengupta, A., Quiaoit, K., Thompson, R. T., Prato, F. S., Gelman, N. and Goldhawk, D.E., *Biophysical features of MagA expression in mammalian cells: implications for MRI contrast.* Frontiers in Microbiology, 2014. **5**.

33. Goldhawk, D., Lemaire, Claude., McCreary, Cheryl R., McGirr, Rebecca., Dhanvantari, Savita., Thompson, Terry R., Figueredo, Rene., Koropatnick, Jim., Foster, Pula. and Prato, Frank S., *Magnetic resonance imaging of cells overexpressing MagA, an endogenous contrast agent for live cell imaging.* Mol Imaging, 2009. **8**: p. 129-139.

34. Zurkiya, O., Chan, A.W., and Hu, X., *MagA is sufficient for producing magnetic nanoparticles in mammalian cells, making it an MRI reporter.* Magn Reson Med, 2008. **59(6)**: p. 1225-1231.

35. Rohani, R., Figueredo, R., Bureau, Y., Koropatnick, J., Foster, P., Thompson, T., Prato, F.S., and Goldhawk, D.E., *Imaging Tumor Growth Non-invasively Using Expression of MagA or Modified Ferritin Subunits to Augment Intracellular Contrast for Repetitive MRI.* Mol Imaging Biol., 2013.

36. Kim, T., Momin, E., Choi, J., Yuan, K., Zaidi, H., Kim, J., Park, M., Lee, N., Mcmahon, M., Quinones-Hinojosa, A. and Bulte, J., *Mesoporous silica coated hollow manganese oxide nanoparticles as positive T1 contrast agents for labeling and MRI tracking of adipose-derived mesenchymal stem cells.* J Am Chem Soc, 2011. **133**: p. 2955-2961.

37. Renier, C., Vogel, H., Offor, O., Yao, C. and Wapnir, I., *Breast cancer brain metastases express the sodium iodide symporter.* J Neurooncol, 2010. **96**: p. 331-336.

38.   Tanaka, M., Mazuyama, E., Arakaki, A. and Matsunaga, T., *MMS6 protein regulates crystal morphology during nano-sized magnetite biomineralization in vivo.* J Biol Chem, 2011. **286(8)**: p. 6386-6392.

39.   Arakaki, A., Webb, J. and Matsunaga, T., *A novel protein tightly bound to bacterial magnetic particles in Magnetospirillum magneticum strain AMB-1.* J Biol Chem, 2003. **278(10)**: p. 8745-8750.

40.   Zhang, X., Robledo, B., Harris, S. and Hu, X., *The magnetosome membrane protein Mms6 produces MR contrast in vitro.* in *19th ISMRM Annual Meeting & Exhibition.* 2011. Montreal, Canada.

41.   Nishimura, D.G., in *Physics in Principles of magnetic resonance imaging.* 1995: Stanford University: Stanford, CA. . p. 55-66.

42.   Haacke, E.M., in *Magnetic Resonance Imaging: physical principles and sequence design.* 1999, J. Wiley-Liss; : New York: . p. 1-16.

43.   Williams, L.A., Gelman, Neil., Picot, Paul A., Lee, David S., Ewing, James R., Han, Victor K. and Thompson, R. Terry., *Neonatal Brain: Regional Variability of in Vivo MR Imaging Relaxation Rates at 3.0 T—Initial Experience.* Radiology, 2005. **235**: p. 595-603.

44.   Westbrook, C., Roth, C.K. and Talbot, J. , *Pulse sequences, MRI in practice.* . June 2005: Wiley-Blackwell.

45.   McRobbie, Donald W., Moore, Elizabeth A., Graves, Martin J. and Prince, Martin R. *MRI From Picture to Proton*. 2006.

46.   Gelman, N., Gorell, J., Barker, P., Savage, R., Spickler, E., Windham, J. and Knight, R., *MR imaging of human brain at 3.0 T: preliminary report on 15 transverse relaxation rates and relation to estimated iron content.* Radiology, 1999. **210**: p. 759-767.

Chapter 2

2 Relaxation Rate Measurements in MagA-expressing Cancer Cells

2.1 Introduction

This chapter presents an investigation of the transverse ($R2^*$, $R2$ and $R2'$) and longitudinal ($R1$) relaxation rates in MagA-expressing MDA-MB-435 cells measured with 3 Tesla (T) MRI. These measurements provide quantitative information on the influence of the iron label on the MRI signals. In addition, elemental iron content measurements are presented and related to the MRI results. The findings highlight the utility of a single magnetotactic bacterial gene as an MR contrast agent. The potential for further improvements in MR detection of gene-based contrast upon a more complete representation

of the magnetosome compartment is predicted.

2.2   Methods

2.2.1 Cell Culture

The cell lines used for these experiments consisted of human MDA-MB-435 in the

form of a clonal population previously transfected with MagA and stably expressing this

gene[1]. Cells were kept in culture for approximately 3 months.

Cells were cultured in low glucose Dulbecco's Modified Eagle Medium

supplemented with 10% fetal bovine serum and 0.5% penicillin/streptomycin. Iron-

supplemented cells were prepared by incubation with medium containing 250 μM ferric

nitrate (Sigma-Aldrich, Oakville, Canada) for at least 5 days. All cell culture reagents were

purchased from Life Technologies (Burlington, Canada) unless otherwise noted.

Each cell type was grown as a monolayer on 100mm-plates. Stable expression of a

MagA clone from pcDNA3.1Zeo(+) was obtained with 800 μg/ml Zeocin. The cultures were

incubated at 37°C until the cells reached 90-100% confluency at which time they were

amplified onto 150mm-culture dishes. At harvest, cells were washed 3 times with

phosphate-buffered saline pH 7.4 (PBS) , a physiological salt solution containing NaCl, KCl,

Na_2HPO_4 and KH_2PO_4 in concentrations of 137, 2.7, 10 and 2 mmol/L respectively, to

remove medium and the extracellular iron supplement. All cell types were harvested from

150 mm plates into centrifuge tubes by gentle trituration and were subjected to three cycles

of centrifugation at 400xg (where "g" stands for relative centrifugal force) for 5 min at 15˚C

during the PBS washes. Cells were then counted using a hemacytometer.

2.2.2 Phantom Preparation

Approximately 50-60 million cells of each type were placed in the wells from a 96-

well break-apart plate (Nunc, Rochester, U.S.A.). Each well of inner diameter 6 mm and

height 10 mm was centrifuged at $400 \times g$ and for 5 min. to form a compact pellet

approximately 6 mm in height. Cell pellets were overlaid with 1% gelatin/PBS and

embedded in one hemisphere of a 9cm spherical phantom filled with 4% gelatin/PBS. A

spherical-shaped phantom was used to minimize macroscopic magnetic field

inhomogeneities which would interfere with accurate $R2'$ measurement. Samples

consisted of either parental or MagA-expressing cells, cultured in the presence and

absence of iron supplementation. To form the spherical gelatin phantom, the empty

hemisphere was filled with 2% gelatin/PBS and placed on top of the half containing cell

samples. To avoid susceptibility artifacts at the interface, air was excluded using a layer of

parafilm. Figure 2.1 illustrates the phantom set-up used for relaxation rate measurements.
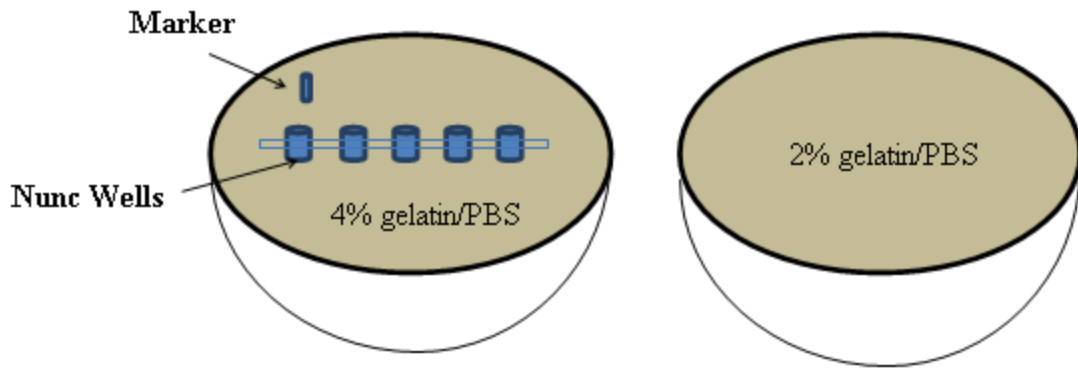
Figure 2.1 Cell Phantom for relaxation rate measurement

2.2.3 Relaxation Rate Measurements

Phantoms were scanned on a 3T Biograph mMR (Siemens AG, Erlangen, Germany) equipped with an actively shielded whole-body gradient system (with maximum gradient strength and slew rate of 45mT/m and 200T/m/s, respectively). A 15-channel knee coil was used for radiofrequency (RF) excitation and signal reception.

Image-based measurements of relaxation rates (R1, R2, R2*) were performed using the sequences and parameters provided in Table 1.

Table 1. Sequences and parameters used for measuring relaxation rates.

Relaxation Rates	Sequence	TE (ms)	TR (ms)	TI (ms)	Matrix	Flip Angle
R2	Single-echo Spin-echo	13-300 (9 TE values)	*1000	-	192×192	90°
R2*	Multi-echo Gradient-echo	6.12-80 (9 echoes)	1000	-	192×192	60°
R1	Inversion-recovery spin-echo	13	4000	22-3900 (6 values)	128×128	90°

*Note: For the single spin-echo sequence rather than fixing TR, the value of TR-TE was fixed ([2] and equation (1.5)).

The slice thickness was 1.5 mm and the field of view (FOV) was 120 mm for all the images.

Voxel dimensions were 1.5×0.6×0.6 mm for R2 and R2* acquisitions and 1.5×0.9×0.9 mm for R1 acquisitions.

MRI data were collected from 11 experiments where each experiment includes cell harvest, phantom preparation and the MRI scan. Typically the phantom for each experiment included four separate samples (i.e. each in a nunc well). In two experiments all cell samples, from each of the four groups [parental(P), iron-supplemented parental (P+Fe), MagA-expressing (MagA) and iron-supplemented MagA-expressing (MagA+Fe)] were

imaged together. Whereas the phantom contained only MagA+Fe and MagA-Fe samples for

six of the experiments and it contained only P+Fe and P-Fe for three experiments.

Image processing and analysis were performed using commercial software tools.

With the aid of MATLAB 7.9.0 (R2010b) a region of interest (ROI) was selected in each

well to include the maximum number of voxels (approx. 30-50), excluding ones adjacent to

the wall of the well. R2, R2* and R1 were determined with least square curve fitting (Sigma

Plot 10.0.inc) of the mean ROI signals using equations 1.5, 1.6 and 1.7 in Chapter 1 as

appropriate where the absolute value of equation 1.7 was used. R2' was obtained by

subtraction (R2*-R2) (refer to equation 1.3 in Chapter 1).

2.2.4 Protein and Trace Element Analysis

Samples were sent to the Analytical Services Laboratory of Surface Science

Western at Western University (London, Canada) for trace element analysis of iron and zinc

using inductively-coupled plasma mass spectrometry (ICP-MS). To prepare samples for trace

element analysis and protein quantification, cells were cultured as described above for MRI

experiments and were harvested based on the confluency of 150mm-culture dishes a day or

two before or after the actual day of MRI scan. Cells were then lysed in

radioimmunoprecipitation assay (RIPA) buffer/protease inhibitor cocktail, such that

approximately 10 million cells were solubilized per ml of lysis solution. The total

protein from lysis of these cultured cells was quantified using the bicinchoninic acid assay

(BCA assay) [3]. Zinc provided a measure of cellular redox status as well as a point of

comparison to amount of iron. Iron content was then normalized to quantity of protein as

determined by the BCA assay . Over the course of relaxation rate measurements, iron content

was periodically evaluated in cultured cells.

2.2.5 Statistical Analysis

Relaxation rate means, standard deviations (SD) and standard errors of the mean

(SEM) were calculated for all group values. We then compared each cell type (parental and

MagA), group mean relaxation rates ($R2^*$, $R2$, and $R2'$) between runs, with versus without

iron supplementation, using the independent sample t-test. We performed analysis of

variance (ANOVA) on the absolute difference values obtained by subtracting mean

relaxation rate values from the respective rank values between groups based on cell type and

iron supplementation. The result showed no significant difference between the mean values.

This was done to test the homogeneity of variance for our non-parametric data. The non-

parametric Kruskal-Wallis test was then used to compare all runs of relaxation rates with iron

versus all runs without iron, combining data from both cell types. Since there is no

accepted method for determining the statistical interaction between two variables with a non-

parametric test a parametric analysis was also performed. (It is the interaction between iron

condition (iron supplemented vs unsupplemented) and cell type (parental vs MagA) that is of

most importance in this study). The parametric test, Two-way ANOVA was run to obtain the

main effects and the interaction between the variables. All tests were two-tailed and SPSS

version 20.0 was the statistical package used. Considering the effects of multiple

comparisons, $p < .01$ was considered as significant. This was based on having 6 comparisons

and rounding off the value 0.05/6 to 0.01. Although there are 4 parameters (R2, R2$'$, R2* and

R1) only 3 are independent (R2, R2$'$ and R2* have only 2 independent parameters) so there

are really only 3x2 = 6 comparisons rather than 4x2 = 8 comparisons.

2.3   Results

2.3.1 Relaxation Rates

Representative spin-echo images of the phantom showing wells containing

parental and MagA-expressing cells are illustrated in Figure 2.2A. Part B of this figure

displays the unnormalized signal decay curves with respect to TE for iron-supplemented

MagA-expressing and parental samples. The symbols represent the mean signal intensities

within regions of interest including most of the voxels in each well as described under

methods. Figure 2.2B shows faster signal decay for iron-supplemented MagA-

expressing cells when compared to the iron-supplemented parental cells.
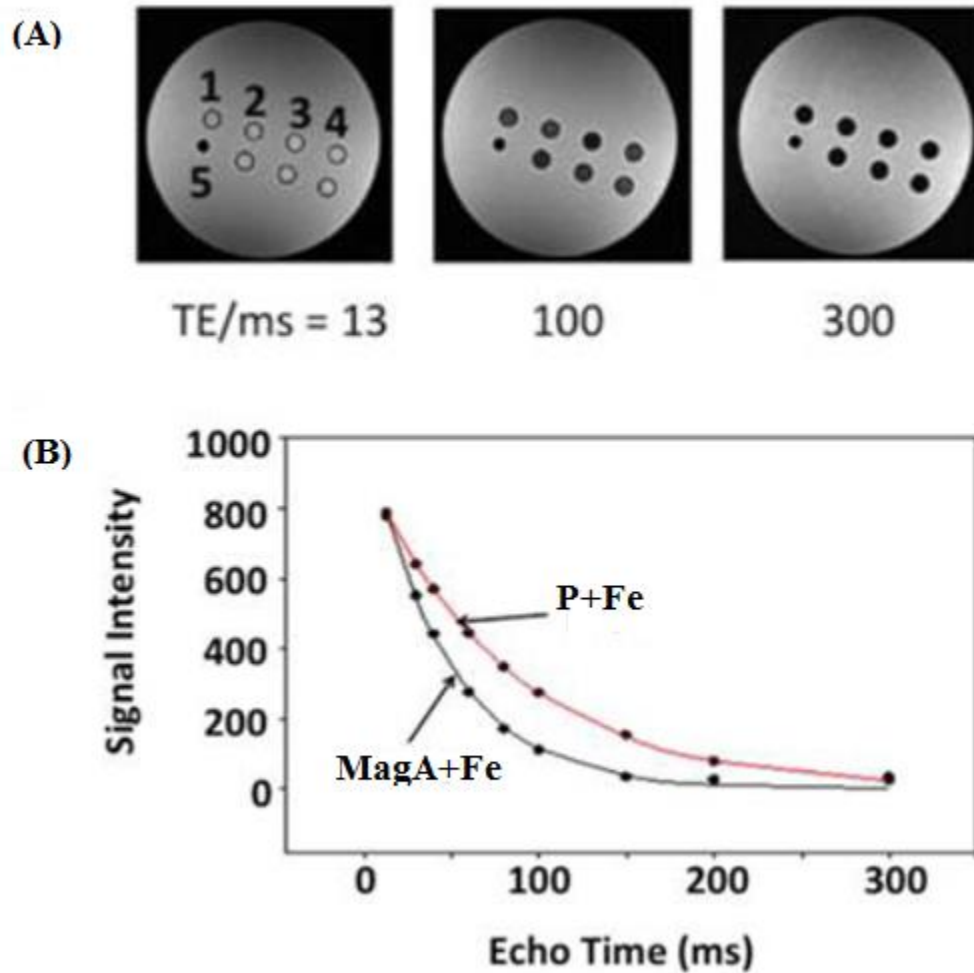
Figure 2.2 Signal decay curves. Representative data indicate the influence of echo time (TE) on signal decay. **(A) Single-echo spin echo (SE) images** show sample wells in cross section at 3 different TE values (13, 100 and 300 ms): 1, parental (P); 2, MagA (A); 3, iron-supplemented MagA (A+Fe); 4, iron-supplemented parental (P+Fe); and 5 polystyrene marker for reference. Samples along the bottom row are combinations of MagA-expressing and parental cells. **(B) R2 relaxation curves are shown for iron-supplemented samples.** Symbols indicate the mean signal intensity within a ROI at each TE. Best fit points are joined by splines to represent an exponential decay.

As expected, $R2^*$ representing the total transverse relaxation rate (comprised of the

reversible component R2$'$ and the irreversible component R2), shows higher decay rate of

signal intensities than its components (Figure 2.3).
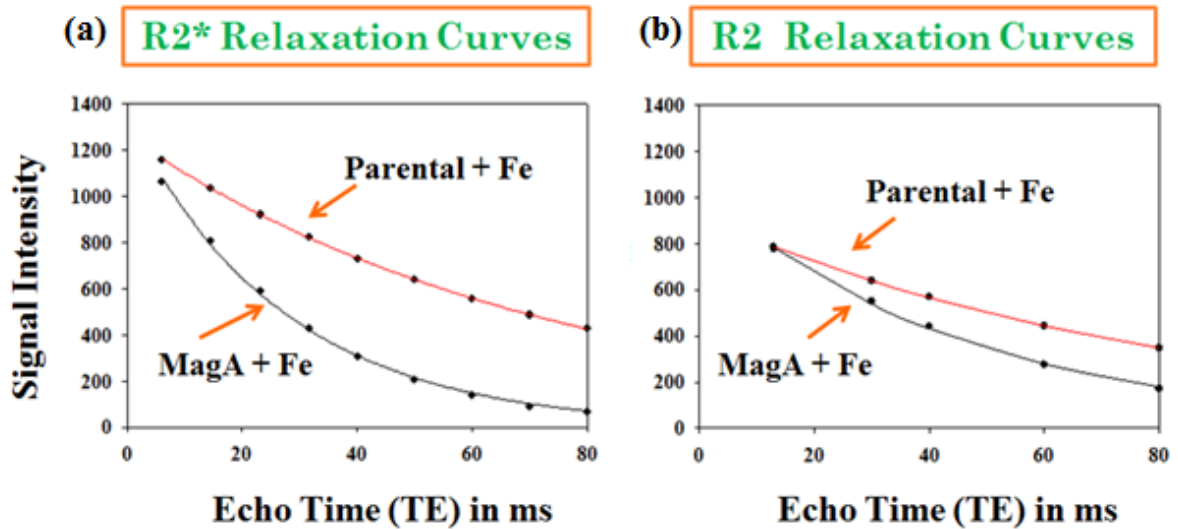
Figure 2.3 Comparison between (a) R2* and (b) R2 relaxation curves for parental and MagA-expressing cell samples. The R2 relaxation curve is the same as Figure 2.2(B), except that it only includes the first 80 ms of the decay for comparison with the R2* curve (a). The R2* curves show a greater difference between the MagA-expressing and parental cells.

Figure 2.3, demonstrates that R2* shows a stronger difference between MagA+Fe and

Parental+Fe than does R2.

Transverse relaxation rates, R2, R2* and R2$'$, all were notably different in

iron-supplemented cells overexpressing MagA. For each relaxation rate, significant main

effects for the iron condition were found with both two-way ANOVA and Kruskal-Wallis

tests (Figure 2.4). More importantly, the ANOVA provided a significant interaction between

iron condition and "cell type", more specifically between iron-supplemented vs.

unsupplemented and MagA-expressing vs. parental.

The independent sample t-test showed that there was no significant difference in

MR relaxation rates for iron-supplemented and unsupplemented parental cells. However, a

statistically significant influence of iron-supplementation existed for $R2^*$ ($p < .01$) and $R2'$

($p < .001$) in cells overexpressing MagA as shown in Figure 2.4. For R2 the influence of iron

supplementation showed only a trend ($p < .05$) when accounting for multiple comparisons.

$R2^*$ provided the greatest absolute difference in MR relaxation rates and $R2'$ displayed the

greatest relative difference. The significant effect of iron supplementation was found also by

the non-parametric Mann-Whitney test.

.
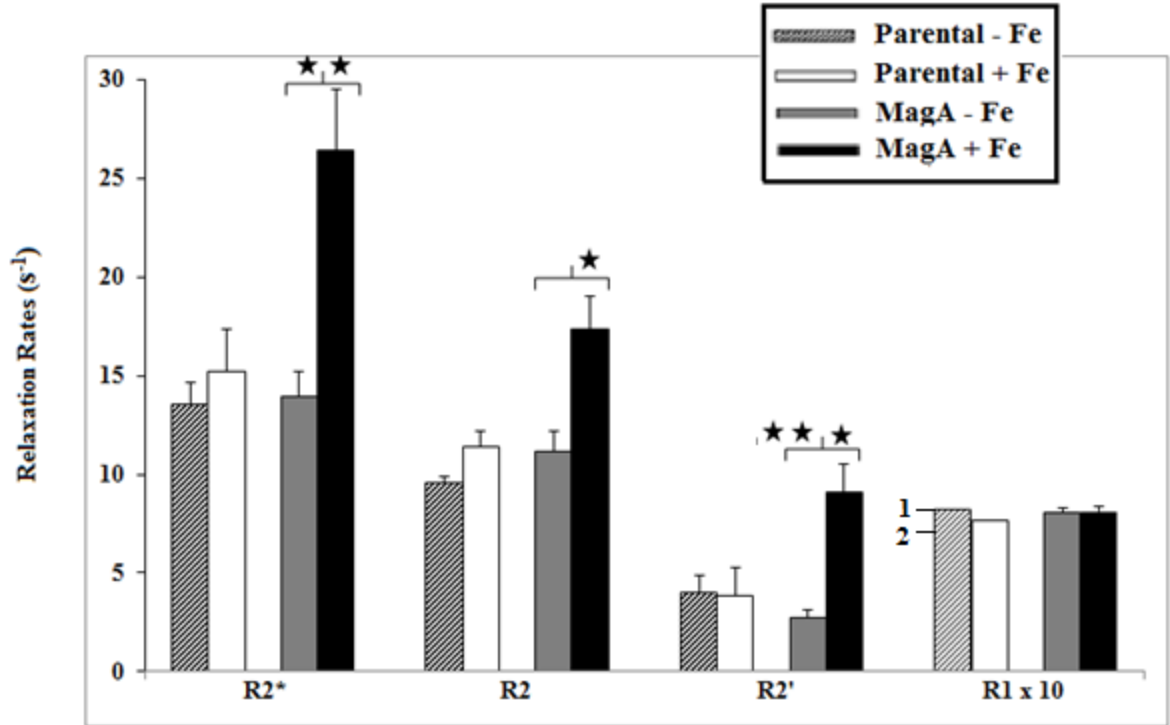
Figure 2.4. Transverse and longitudinal relaxation rates. Bar graphs indicate the change in all 3 transverse relaxation rates and the lack of change in longitudinal relaxation rate upon iron supplementation of parental and MagA-expressing cells. $R2^*$ showed the greatest absolute difference between iron supplemented vs. unsupplemented cells, while $R2'$ showed the greatest relative difference between these cell groups. R1 is similar for all parental (n=2) and MagA-expressing (n=5) cell samples. Error bars represent SEM. The number of samples for parental+Fe, parental-Fe, MagA+Fe, MagA-Fe were 5, 5. 8 and 8 respectively for transverse measurements and 2, 2, 5 and 5 for longitudinal relaxation rate measurents. ★★★ for $p < .001$, ★★ for $p < .01$ and ★ for $p < .05$ (trend).

The bar chart in Figure 2.4 shows the mean values of the transverse and

longitudinal relaxation rates of parental and MagA-expressing cell samples both iron-

supplemented and unsupplemented. Significant differences are observed between $R2^*$

($p < .01$) and $R2'$ ($p < .001$) for iron-supplemented MagA-expressing cells.

42

Figure 2.5 illustrates a scatter plot of the individual transverse relaxation rates for each group. This scatter plot is presented in addition to the bar graph in Figure 2.4 (means and SEMs) in order to more completely show the variability of measurements. Although the transverse relaxation rates for iron-supplemented MagA-expressing cells were significantly higher than for unsupplemented MagA-expressing samples, there is nevertheless substantial variability in measurements especially when iron-supplemented.

For all cell types and culture conditions, R1 remained virtually constant between 0.72- 0.81 s^{-1} and was not pursued as an indicator of cellular iron contrast. The scatter plots for R1 are not shown because variability was low for R1.
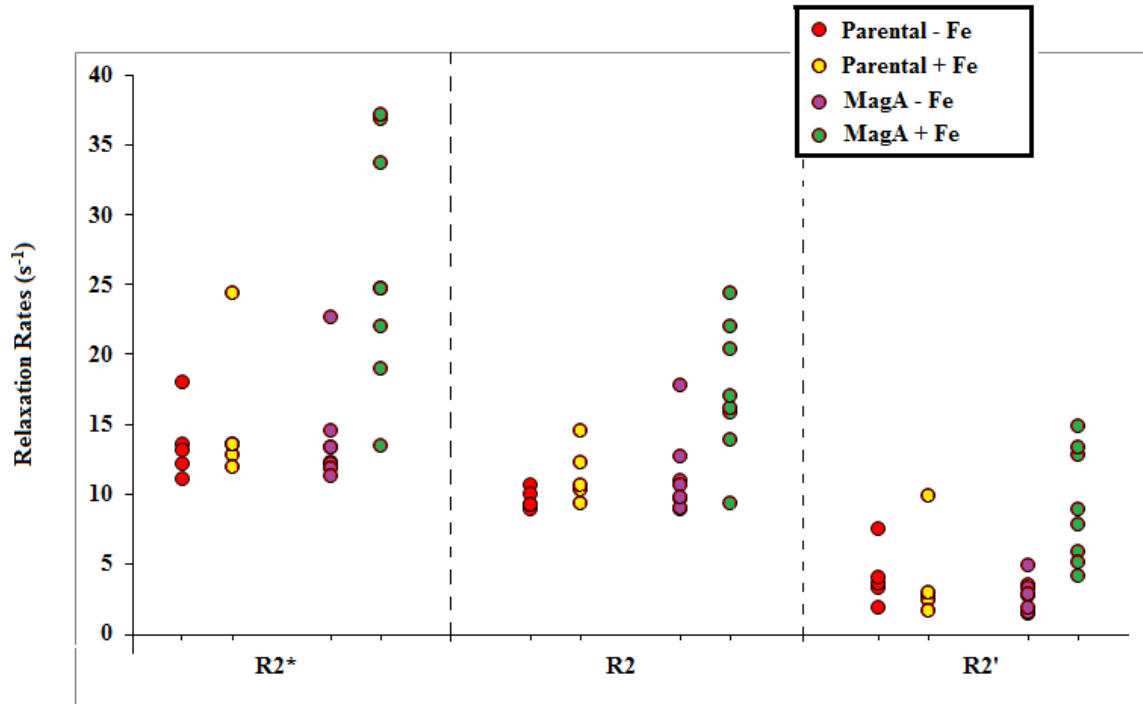
Figure 2.5. Scatter plot showing transverse relaxation rates for parental and MagA-expressing cell samples both iron-supplemented and unsupplemented. This plot was included to illustrate the relatively large degree of variability in these rates especially for iron-supplemented MagA-expressing cells.

2.3.2 Trace Element Measurements

In MagA-expressing cells, cultured in the absence of iron supplementation, ICP-MS analysis indicated 0.047 ± 0.006 µg Fe/mg protein (n=7; mean $\pm$ SEM) and 0.249 ± 0.047 µg Zn/mg protein. In contrast, the presence of iron supplementation in MagA-expressing cells increased iron content to approximately 0.755 ± 0.157 µg/mg protein while level of zinc stayed at approximately 0.135 ± 0.023 µg /mg protein (Table 2). Additional data for the ratio of iron/zinc in non-supplemented cultures showed lower values compared to the

44

supplemented ones. Samples both in presence and absence of iron when evaluated using a

student's t test showed significance at $p < .01$ for iron, but not significant for zinc.

Table 2. Trace element analysis^ of cells cultured in the presence or absence of iron supplementation.*

Sample	Iron[#]	Zinc[#]	Fe/Zn	N
P	0.250	0.117	2.14	1
P+Fe	0.475	0.107	4.44	1
MagA	0.047 ± 0.006	0.249 ± 0.047	0.19	7
MagA+Fe	0.755 ± 0.157	0.135 ± 0.023	5.60	7

^ Data were collected using either ICP-MS.

* Cells were incubated in the presence (+Fe) or absence of 250 μM ferric nitrate

Elemental analysis is reported as μg/mg protein; mean ± SEM in case of MagA-expressing samples only.

Figure 2.6 illustrates a plot of the transverse relaxation rates $R2^{*}$, R2 and $R2^{'}$ vs iron

content, for iron supplemented and unsupplemented MagA-expressing cell samples.

(A)

R2* Relaxation Rates

R² = 0.85

Iron Content (μg / mg protein)

(B)

R2 Relaxation Rates

R² = 0.73

Iron Content (μg / mg protein)
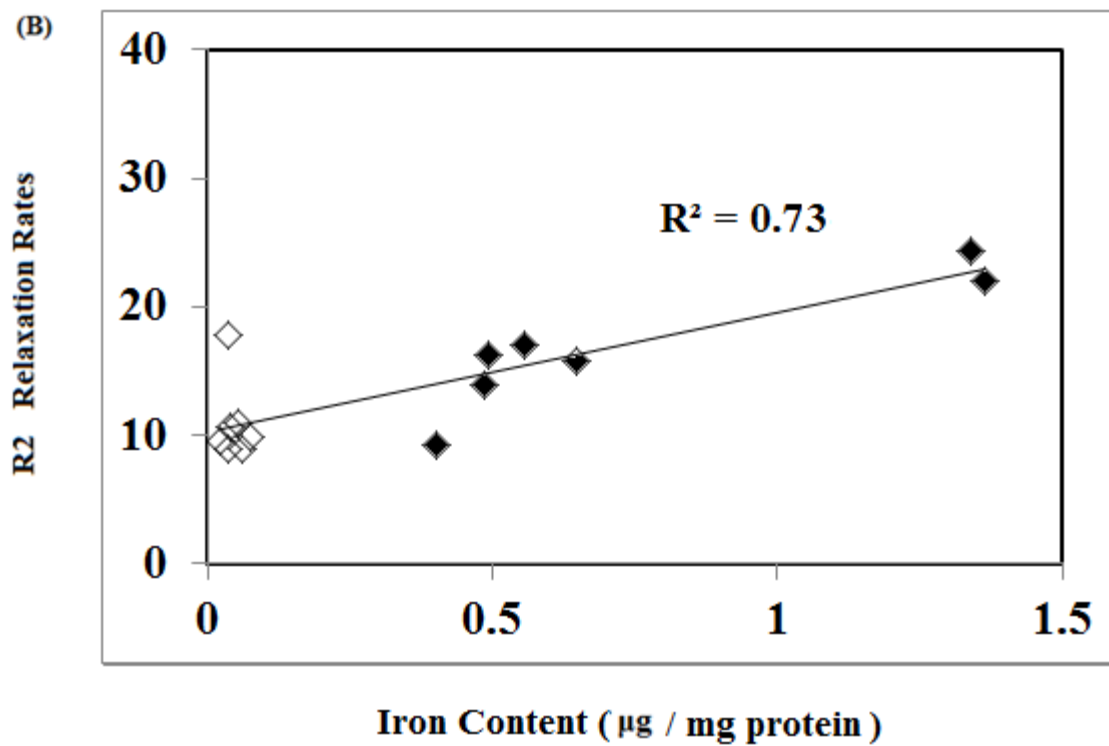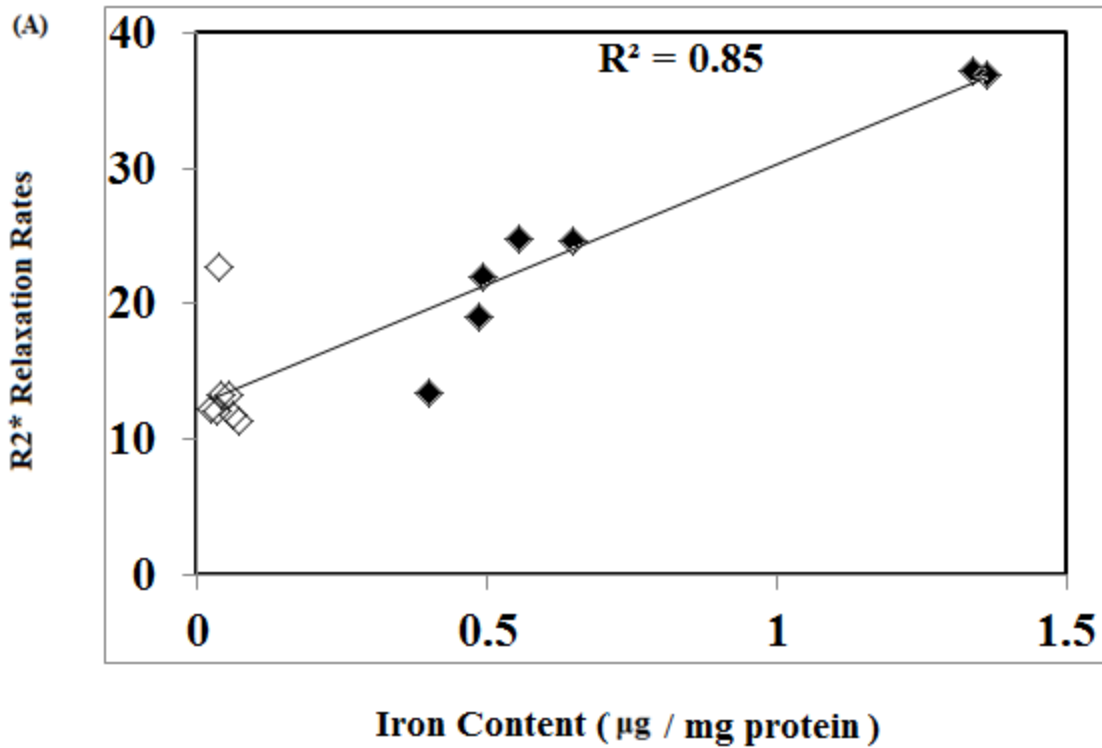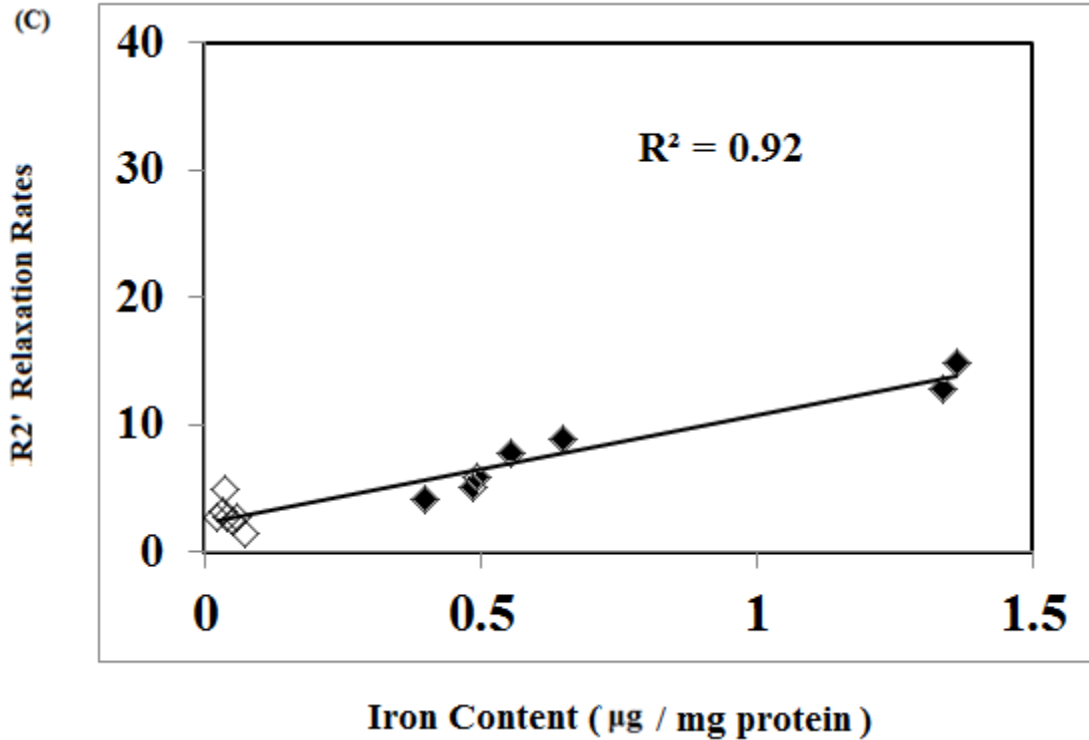
Figure 2.6. Relaxation rates (A) R2*, (B) R2 and (C) R2′ vs iron content for MagA-expressing cell samples. All the graphs showed correlation of relaxation rates with iron content (μg per mg of protein) in MagA-expressing cell samples both iron-supplemented and unsupplemented (empty diamonds = MagA and filled diamonds = MagA+Fe).

As shown in Figure 2.6, a significant correlation ($p < .005$) between R2' and iron content (normalized to protein content) was observed.

2.4 Discussion

The results of this study may help to design and optimize methods for tracking gene-based iron-labeled cells in vivo. Relaxation rate measurements, a quantitative approach to assess iron-related contrast, may be helpful to track iron-loaded cells more precisely in the

developing tumor. As advances in MR hardware, sequences and contrast agents [4] progress,

so too will molecular MRI. In this study, to approach that goal, measurements of relaxation

rates were performed to explore the potential for contrast enhancement in cancer cells

utilizing overexpression of MagA, a bacterial gene.

Using phantoms of compact cell pellets, we quantified cellular MR contrast using

relaxation rate measurements. Longitudinal relaxation rates were influenced very little, if

any, by the cellular iron and this is consistent with the literature [5]. On the other hand,

transverse relaxation rates were strongly affected by iron supplementation for

MagA-expressing cells (Figure 2.4). For this cell type the elemental iron content was also

higher in supplemented versus unsupplemented samples.

Every cell maintains their normal redox states which when disturbed, toxic effects

like oxidative stress occur, damaging components of cells. Changes in cellular zinc levels

provide one indicator of oxidative stress [6]. In our analyses, we showed specific iron uptake

and relatively constant levels of zinc in iron-supplemented MagA-expressing cells, consistent

with little or no redox cytotoxicity.

In this study, the relaxation rates and iron levels for MagA-expressing cells

investigated in presence of iron-supplementation demonstrated the potential for taking up

iron, leading to MRI contrast. This quantitative result was consistent with a previous study

where the potential of MagA-expression to produce intracellular contrast in mouse

neuroblastoma (N2A) cells was studied [1]. As well, the iron-related contribution to

transverse relaxation increases with field strength, thus, contrast differences between gene

expression and controls should be greater at higher fields.

R2 measurements have previously been reported in 293FT cells expressing MagA

(approx. 20 s-1, 3 T, n=4) [7]. The values for MagA-expressing cells compare well

with the findings in this thesis; however, my results (Figure 2.4) indicated that R2 alone

provides the weakest index of MR contrast activity based on student's unpaired t-test.

Measures of $R2^*$ and $R2'$ were found to provide the most statistically significant changes in

cellular contrast upon iron supplementation. In addition, relative changes in $R2'$ were larger

than those in R2, suggesting the potential of $R2'$ for better iron-related specificity, as

previously suggested for human brain regions with high iron [2]. This may be important for

in vivo cell tracking and optimization of molecular MRI.

In our study, the constitutive expression of MagA in MDA-MB-435 cells was

unhampered by protein tags and previously confirmed to provide high levels of MagA

mRNA expression relative to β-actin using reverse transcription polymerase chain reaction

(RT-PCR). The constitutive expression of fusion protein, enhanced green fluorescent protein (EGFP)-MagA, has been confirmed in both mouse neuroblastoma N2A cells [1] and in MDA-MB-435 cells (unpublished results). Using the MTT assay, it has also been shown that the proliferation of transfected tumor cells is not altered by the activities of MagA expression [1]. In our study we detected the activity of MagA using relaxation rate measurements. In addition, iron uptake in MagA-expressing cells was greatly influenced by the presence of an iron supplement (250 μM ferric nitrate).

In a mouse xenograft model of tumor growth, Rohani et al. [8] showed that MagA expression generated a peak in MR contrast in vivo during the second week of tumor growth, similar to the contrast derived from the expression of modified ferritin subunits lacking iron response elements to enable continuous expression. Beyond 3 weeks post-injection, MR contrast in the parental tumor also increased, reducing the benefit of contrast gene expression in larger tumors. To improve image analysis, relaxation rate measurements using optimal measures provides an additional tool for assessing MagA-derived MR contrast and could be implemented for a longitudinal study as that by Rohani et. al.[8].

Gene-based contrast like MagA overexpression may be helpful in tracking metastasis in the white matter of brain for breast cancer [9]. When a gene-based iron contrast

responds clearly to iron supplementation, it becomes suitable for revealing changes in iron

homeostasis. As an example, in a study by Shpyleva et al., they reported changes in the level

of ferritin subunits between epithelial and mesenchymal breast tumor cell lines [10]. In that

study MagA overexpression might be a preferred tool to track cells in order to avoid

interference with the cell biology related to cancer.

The finding of this work that relaxation rates for MagA-expressing cells can be

distinguished from parental controls is encouraging, however for *in vivo* detection the

challenge will be to distinguish MagA-expressing cells from surrounding tissue. In vivo there

is an additional challenge of distinguishing MagA-expressing iron labeled cells from

endogenous iron, where the level of endogenous iron will depend on the particular organ to

be imaged. For in vivo image acquisition, relaxation rate measurements will encounter

further limitations. Background field inhomogeneities due to susceptibility differences

between tissues will always contribute to $R2^*$ measurements unless correction procedures are

applied [11]. Furthermore, the measurement of R2 would require long acquisition times.

Although transverse relaxation rates vary as a function of tissue iron [12],

R2 in particular is affected by other factors in the tissue or cell, such as water content

reflecting proton density, subcellular compartmentalization and water-protein interactions.

By comparison, $R2'$ is mostly influenced by sources of magnetic field inhomogeneity. If

sources of macroscopic inhomogeneity are minimized, as done here by using a spherical

phantom, then $R2'$ should be influenced mostly by microscopic sources of inhomogeneity,

which in our samples should be from iron particles. In order to correct for macroscopic

inhomogeneities in-vivo, post processing methods have been developed [11]. This involves

the use of the phase of the gradient echo signals, for which no added acquisition is required.

In a study on small animal imaging this same idea was adapted where $R2^{*}$ and $R2'$

measurements from superparamagnetic iron nanoparticles labeled cancer cells were reported

[11].

The results reflected in Figure 2.6, supported the notion that transverse relaxation

rates are strongly influenced by the amount of iron [2]. Among all the transverse relaxation

rates, $R2'$ showed the strongest correlation with the amount of iron for MagA-expressing

cells. This suggests the potential of $R2'$ for better iron-related specificity for imaging of

gene-based iron-labeled cells and is consistent with, the effect of iron in human brain regions

with high iron [2].

From our iron level measurements expressed as µg Fe/mg protein we can estimate

the amount of iron per cell in our samples. Our nunc wells had approximately 60×10^{6} cells

in a volume of $\pi(3mm)^2$ (6 mm) $\approx$ 170 μL, and this corresponds to 3×10^{-9} g/cell assuming a

density of 1.0 g/ml. If we also assume that approximately 20% of the mass of a cell is protein

then each cell has approximately 6×10^{-7} mg protein/cell. Therefore our highest iron level for

MagA+Fe ($\approx$1.4 μg Fe/mg protein) corresponds to approximately 0.84 pg Fe/cell which is

similar to the levels reported by Zurkiya et al [7] ($\approx$0.6 μg Fe/cell) and almost 100 times

smaller than reported for SPIO loading [13]. The number of cells in each MRI voxel

can be estimated from the number of cells/volume (60×10^6 /170 μL) and the volume of each

voxel ($\approx$0.5 μL) leading to an estimate of $\sim 2 \times 10^5$ cells/ voxel. In a separate report [20] we

demonstrated voxel-by-voxel mapping of these relaxation rates indicating that we can easily

detect 2×10^5 cells with this setup. However our phantom included approximately 400g of gel

which acted as a large source of noise. If we were imaging a mouse brain for example ($\sim$10 g)

inside a small RF coil we would have greatly increased signal-to-noise and could detect

perhaps $\sim 10^4$ cells and perhaps as low as 10^3 cells especially at higher field strength and with

more optimized acquisitions.

The principle iron import mechanism in mammals, via the transferrin receptor, is

universally expressed in almost all cells [14], with increased levels of transferrin expression

in cells that are propagating rapidly and require iron in order to function [15]. Tumor cells

when compared to healthy tissue have low levels of ferritin expression with high levels of

transferrin receptor[16, 17]. These changes related to iron uptake regulation, storage and

distribution support rapid cell proliferation, for example by supplying iron as a cofactor for

ribonucleotide reductase and DNA synthesis [18, 19]. The propensity of proliferating cells

toward iron uptake may be used to best advantage in cancer cell tracking by MRI and the

development of gene-based contrast. In a related study from my work, a drop in transferrin

receptor was detected in parental (data not shown) as well as engineered cells following

culture in the presence of iron supplementation [20]. Therefore, the activity of MagA has

elicited the same homeostatic response as expected of an increase in ferritin storage. In spite

of this, a statistically significant level of MR contrast enhancement was achieved suggesting

that MagA may function outside the regulatory control of iron binding proteins. In the case of

MagA activity, the lack of cellular regulation may be reflected in greater fluctuation in iron

levels and therefore in MR contrast. This in turn may result in a relatively large degree of

variability in the transverse relaxation rates of the iron-supplemented MagA-expressing cells

(Figure 2.5). The ability of MagA to circumvent key features of mammalian iron regulation,

without causing cytotoxicity, will bode well for future development of gene-based contrast.

2.5   References

1. Goldhawk, D., Lemaire, Claude., McCreary, Cheryl R., McGirr, Rebecca., Dhanvantari, Savita., Thompson, Terry R., Figueredo, Rene., Koropatnick, Jim., Foster, Pula. and Prato, Frank S., *Magnetic resonance imaging of cells overexpressing MagA, an endogenous contrast agent for live cell imaging.* Mol Imaging, 2009. **8**: p. 129-139.

2. Gelman, N., Gorell, J., Barker, P., Savage, R., Spickler, E., Windham, J. and Knight, R., *MR imaging of human brain at 3.0 T: preliminary report on 15 transverse relaxation rates and relation to estimated iron content.* Radiology, 1999. **210**: p. 759-767.

3. Smith, P., Krohn, R., Hermanson, G., Mallia, A., Gartner, F., Provenzano, M., Fujimoto, E., Goeke, N., Olson, B. and Klenk, D., *Measurement of protein using bicinchoninic acid.* Anal Biochem,, 1985. **150**: p. 76-85.

4. Huang, J., Zhong, X., Wang, L., Yang, L. and Mao, H., *Improving the magnetic resonance imaging contrast and detection methods with engineered magnetic nanoparticles.* Theranostics, 2012. **2**: p. 86-102.

5. Bin Na, H., Song, I. and Hyeon, T., *Inorganic nanoparticles for MRI contrast agents.* Adv Mater, 2009. **21**: p. 2133-2148.

6. Chung, M., Hogstrand, C. and Lee, S.-J., *Cytotoxicity of 1 nitric oxide is alleviated by 2 zinc-mediated expression of antioxidant genes.* Exp Biol Med, 2006. **231**: p. 1555-1563.

7. Zurkiya, O., Chan, A.W., and Hu, X., *MagA is sufficient for producing magnetic nanoparticles in mammalian cells, making it an MRI reporter.* Magn Reson Med, 2008. **59(6)**: p. 1225-1231.

8. Rohani, R., Figueredo, R., Bureau, Y., Koropatnick, J., Foster, P., Thompson, T., Prato, F.S., and Goldhawk, D.E., *Imaging Tumor Growth Non-invasively Using Expression of MagA or Modified Ferritin Subunits to Augment Intracellular Contrast for Repetitive MRI.* Mol Imaging Biol., 2013.

9. Renier, C., Vogel, H., Offor, O., Yao, C. and Wapnir, I., *Breast cancer brain metastases express the sodium iodide symporter.* J Neurooncol, 2010. **96**: p. 331-336.

10. Shpyleva, S., Tryndyak, V., Kovalchuk, O., Starlard-Davenport, A., Chekhun, V., Beland, F. and Pogribny, I., *Role of ferritin alterations in human breast cancer cells.* Breast Cancer Res Treat, 2011. **126**: p. 63-71.

11. Kuhlpeter, R., Dahnke, H., Matuszewski, L., Persigehl, T., Von Wallbrunn, A., Allkemper, T., Heindel, W., Schaeffter, T. and Bremer, C., *R2 and R2* Mapping for*

Sensing Cell-bound Superparamagnetic Nanoparticles: In Vitro and Murine in Vivo Testing. Radiology, 2007. **245**: p. 449-457.

12. Wood, J., Enriquez, C., Ghugre, N., Tyzka, J., Carson, S., Nelson, M. and Coates, T., *MRI R2 and R2* mapping accurately estimates hepatic iron concentration in transfusion-dependent thalassemia and sickle cell disease patients.* Blood, 2005. **106**: p. 1460-1465.

13. Heyn, C., Ronald, J.A., Mackenzie, L.T., MacDonald, I.C., Chambers, A.F., Rutt, B.K., and Foster, P.J., *In vivo magnetic resonance imaging of single cells in mouse brain with optical validation.* Magnetic Resonance in Medicine, 2006. **55**: p. 23-29.

14. Ponka, P., and Lok, C., *The transferrin receptor: Role in health and disease.* Int J Biochem Cell Biol, 1999. **31**: p. 1111-1137.

15. Pantopolous, K., Porwal, S., Tartakoff, A. and Devireddy, L. , *Mechanisms of mammalian iron homeostasis.* Biochemistry, 2012. **51**: p. 5705-5724.

16. Anderson, C., Shen, M., Eisenstein, R. and Leibold, E. , *Mammalian iron metabolism and its control by iron regulatory proteins.* Biochem Biophys Acta, 2012. **1823**: p. 1468-1483.

17. Daniels, T., Delgado, T., Rodriguez, J., Helguera, G. and Penichet, M., *The transferrin receptor part I: biology and targeting with cytotoxic antibodies for the treatment of cancer.* Cl Immunol, 2006. **121**: p. 144-158.

18. Nyholm, S., Mann, G., Johansson, A., Bergeron, R., Graslund, A. and Thelander, L., *Role of ribonucleotide reductase in inhibition of mammalian cell growth by potent iron chelators.* J Biol Chem, 1993. **268**: p. 26200-26205.

19. Weinberg, E., *Roles of iron in neoplasia. promotion, prevention, and therapy.* Biol Trace Element Res, 1992. **34**: p. 123-140.

20. Sengupta, A., et al., *Biophysical features of MagA expression in mammalian cells: implications for MRI contrast.* Frontiers in Microbiology, 2014. **5**(29).

Chapter 3

Summary and Future work

3.1   Summary of Findings

In summary, we have used the *MagA* gene from magnetotactic bacteria to impart

magnetic sensitivity to mammalian cancer cells and provide groundwork for cell tracking by

MRI. Our study reported the use of transverse relaxation rate measurements as an effective

tool for quantifying the contrast enhancement previously reported [1] in MDA-MB-435 cells

overexpressing MagA, under iron supplemented conditions. Although transverse relaxation

rate measurements revealed an increased value for iron-supplemented MagA-expressing cells

compared to its unsupplemented and parental controls, longitudinal relaxation rates failed to

discriminate between these cell types regardless of the level of extracellular iron. Also R2'

quantification of MagA-expressing iron-labeled cells showed a potential to be more

characteristic of iron, consistent with previous studies of tissue and suggesting that R2' has

better iron-related specificity than other relaxation rates [2].

Our results also suggested a relatively large degree of variability in both transverse

relaxation rate and the intracellular iron content of MagA-expressing cells cultured in the

presence of iron supplementation. Further work to determine the sources of variability will

increase the potential of R2' as an indicator of MagA-derived contrast and may provide gene-based contrast for MRI which in future may help to detect cell growth and differentiation more effectively in vivo.

3.2   Future Work

Chapter 2 establishes a method of detecting gene-based iron-labeled cells in-vitro through quantifying the MRI signal changes associated with cellular iron uptake by MagA-expressing cells. A natural extension of this work would be its implementation for cell-tracking in-vivo such as in the case of a mouse model of tumour growth from transplanted cells [1]. Previously reported methods [3] for correcting $R2'$ for "macroscopic" magnetic field inhomogeneities within tumor tissue, where the iron-related contributions to R2' are expected to be minimal can be implemented and tested in the absence of iron supplementation. There are some challenges related to R2 and $R2'$ measurements in vivo with R2 requiring long acquisition times unless a multi-echo acquisition is used and $R2'$ being influenced mostly by magnetic field inhomogeneties that can be corrected with the use of the phase of the gradient echo signals. Also, relaxation mapping reported recently [4] using optimal measures provides an additional tool for improving image analysis. R2 and $R2'$ these

measurements can also be performed in mice bearing subcutaneous tumors on the hind limb expressing MagA. In that case parental tumors on the opposite flank may provide physiologically-relevant controls. Based on the results of this thesis, it can be hypothesized that both R2 and R2′ values will be higher in MagA-expressing tumors than in controls, and that the relative differences between MagA-expressing and parental cells will be higher for R2′.

This study can be extended for repetitive imaging of tumor growth and metastasis in small animal model, with the goal of tracking changes in relaxation rates longitudinally with time. In this instance, utilization of a MagA construct tagged with the hemagglutinin (HA) epitope and commercial antibodies, will be suitable to correlate regions within the tumor exhibiting MR contrast with localization of HA-MagA-expressing cells. The potential of a dietary iron supplement for improving tumor cell contrast can also be examined.

In this particular thesis all the MR measurements were done at 3T. Previous studies showed that $R_2′$ in tissue increased with field strength [2], suggesting that stronger $R_2′$ differences between MagA and parental or other cells or tissues will be found at higher fields. Thus for implementation of relaxation measurements for in-vivo tracking may be better at higher fields.

In mammalian cells, effective MR contrast derived from the overexpression of

iron handling protein(s) would benefit from a better understanding of which combination of

magnetotactic bacterial genes will (1) sequester iron within a membrane-enclosed vesicle and

(2) allow biomineralization of iron in the presence of mammalian iron homeostasis.

Magnetosome gene knock-out studies [5] suggests the probability that a subset of genes may

be used to generate a minimal compartment in multiple cell types that would permit iron

biomineralization for non-invasive medical imaging with MRI.

Is it possible for magnetosome-like particles to be reproduced in mammalian cells

in a safe and efficient manner for biomedical molecular imaging? Further research on

magnetotactic bacteria will provide critical information upon which this question may be

judged. Taking current knowledge into consideration, magnetosome-like vesicles in

eukaryotic cells should a) be composed of a lipid bilayer that interacts with cytoskeletal

protein to impart stability, b) be exposed to cytoplasmic or extracellular precursors for

biomineralization, c) impart magnetic properties to the cell, and d) be non-essential for cell

survival. The strict regulation of iron in vivo is advantageous in several ways, permitting

genetic manipulation of its localization, crystallization and association with key cellular

processes. We need additional information regarding prokaryotic iron binding proteins

that can be genetically engineered to handle iron in a eukaryotic environment. We also need

to understand more about magnetic particles in mammalian and vertebrate systems.

The manner in which magnetite is dismantled during cell turnover or when magnetosome-

like reporter gene expression is turned off will be important to understand for effective

measurement of cell tracking and of cellular activity. In principle, regulation of crystal size

and shape should influence MRI. However, recreating magnetism whereby cells move in a

magnetic field is not necessarily the goal of MR contrast. For medical imaging, we may not

need to form the same single magnetic domain that magnetotactic bacteria require for

magnetotaxis. This function requires larger magnetite crystals, approximately 50-100 nm in

length and their alignment along the magnetosome filament [6]. Crystal sizes that induce

superparamagnetic properties are approximately 30 nm in length and suitable for MRI and

altering proton spins. While an elaborate set of reactions and protein-protein interactions

contributes to the formation of uniform magnetite crystals, some redundancy in the protein

architecture of magnetosomes raises the possibility that a more basic set of magnetosome

genes might be sufficient for iron biomineralization and compartmentalization within a lipid

vesicle. Understanding the role of each magnetosome gene will foster future pre/clinical

applications in MRI.

Development of these non-invasive cellular imaging methods is relevant to the study

of cancer progression. Preclinical models of aggressively growing cancers may be assessed

sooner in their development with respect to size or the change in cellular activity using

MagA overexpression as a tool. In future, this could potentially be applied to small animal

MRI to examine *MagA* reporter gene expression in developing tumor.

3.3 References

1.   Rohani, R., Figueredo, R., Bureau, Y., Koropatnick, J., Foster, P., Thompson, T., Prato, F.S., and Goldhawk, D.E., *Imaging Tumor Growth Non-invasively Using Expression of MagA or Modified Ferritin Subunits to Augment Intracellular Contrast for Repetitive MRI.* Mol Imaging Biol., 2013.

2.   Gelman, N., Gorell, J., Barker, P., Savage, R., Spickler, E., Windham, J. and Knight, R., *MR imaging of human brain at 3.0 T: preliminary report on 15 transverse relaxation rates and relation to estimated iron content.* Radiology, 1999. **210**: p. 759-767.

3.   Kuhlpeter, R., Dahnke, H., Matuszewski, L., Persigehl, T., Von Wallbrunn, A., Allkemper, T., Heindel, W., Schaeffter, T. and Bremer, C., *R2 and R2* Mapping for Sensing Cell-bound Superparamagnetic Nanoparticles: In Vitro and Murine in Vivo Testing.* Radiology, 2007. **245**: p. 449-457.

4.   Sengupta, A., Quiaoit, K., Thompson, R. T., Prato, F. S., Gelman, N. & Goldhawk, D.E., *Biophysical features of MagA expression in mammalian cells: implications for MRI contrast.* Frontiers in Microbiology, 2014. **5**(29).

5.   Greene, S., and Komeili, A., *Biogenesis and subcellular organization of the magnetosome organelles of magnetotactic bacteria.* Curr Opin Cell Biol, 2012. **24**: p. 490-495.

6.   Goldhawk, D., Rohani, R., Sengupta, A., Gelman, N. and Prato F., *Using the magnetosome to model effective gene-based contrast for magnetic resonance imaging.* WIRES Nanomed Nanobiotechnol, 2012. **4**: p. 378-388.

Appendix I

Curriculum Vitae

Anindita Sengupta

Room E5-128 Lawson Health Research Institute,
St. Joseph's Health Care, 268 Grosvenor St., London, ON, Canada N6A 4V2

EDUCATION

05/12 – 06/14	**M.Sc. in Medical Biophysics**
	University of Western Ontario, London, Ontario
	Supervisors: Neil Gelman, PhD and Donna Goldhawk, PhD
	Advisors: Terry Thompson, PhD and Lisa Hoffman, PhD
	Research Project: "MRI Relaxation Rates: A Quantitative Approach to Track Tumour Cells Expressing MagA."
08/07 – 12/09	**M.S. in Physics**
	Indiana University of Pennsylvania, Indiana, PA, USA
	Supervisor: Feng Zhou, PhD
	Thesis: "A Fiber-Optic Q-Switch Based On Electro-optic Ceramic For Q-Switched Fiber Lasers"
02/05 – 01/06	**B.Ed. in Education**
	University of Calcutta, West Bengal, India
05/98 – 05/02	**B.Sc. (Honors) in Physics**
	University of Calcutta, West Bengal, India

SCHOLARSHIPS AND AWARDS

05/12 – 04/14	Western Graduate Research Scholarship (WGRS)
	University Of Western Ontario, London, ON
08/07 – 12/09	Graduate Assistanceship
	Indiana University of Pennsylvania, Indiana, PA, USA
2008	Honored Graduate Student Award for Research Poster Presentation
	Indiana University of Pennsylvania, Indiana, PA, USA

WORK EXPERIENCE

09/11 – 04/12	Research Assistant under Dr. Neil Gelman and Dr. Donna Goldhawk
	Lawson Health Research Institute, Imaging Program, London,ON

- *MRI sequence optimization, data acquisition and analysis.*
- *Development of MRI application in molecular imaging.*

64

- *Cell Culture*
- *Collected data using MRI for cell imaging research.*

08/07 – 12/09　　　　Graduate Teaching Assistant
Department of Physics, Indiana University of Pennsylvania, Indiana, PA, USA

- *Tutored undergraduate students for lab work in introductory courses and helped them to solve class assignments.*
- *Presented research work through thesis defense, poster presentation and projects to large audiences.*
- *Applied programming skills to solve problems in physics using database, object oriented and simulation software.*
- *Assisted faculty members in their research work and helped them in grading lab reports.*

PUBLICATION

1. **Sengupta, A.**, Quiaoit, K., Thompson, R. T., Prato, F. S., Gelman, N. & Goldhawk, D.E., *Biophysical features of MagA expression in mammalian cells: implications for MRI contrast.* Frontiers in Microbiology, 2014. **5**(29).
2. Goldhawk, D., Rohani, R., Sengupta, A., Gelman, N., & F.S. Prato. *Using the magnetosome to model effective gene-based contrast for magnetic resonance imaging.* Rev. Nanomed. Nanobiotechnol. 4: 378-388 (2012) - [Published PMID: 22407727]

PRESENTATIONS

POSTERS:

1. **Sengupta, A**., Thompson, R.T., Prato, F.S., Goldhawk, D., & N. Gelman. Irreversible and Reversible Transverse Relaxation Rates Alter with Fractional Volume of MagA-expressing Cancer Cells *London Health Research Day,* London, Ontario, Canada, March 19, 2013.
2. **Sengupta, A**., Rohani, R., Thompson, R.T., Prato, F.S., Goldhawk, D., & N. Gelman. Transverse and Longitudinal MRI Relaxation Rates in MagA-expressing Human Cancer Cells. World Molecular Imaging Conference, Dublin, Ireland, September 5-8, 2012.
3. **Sengupta, A**., Rohani, R., Thompson, R.T., Prato, F.S., Goldhawk, D., & N. Gelman. Iron Labeling of Human Cancer Cells with the MagA Reporter Gene Leads to Increased MRI Relaxation Rates. *London Imaging Discovery Conference, London, Ontario, Canada,* June 27, 2012.
4. **Sengupta, A**., Rohani, R., Thompson, R.T., Prato, F.S., Goldhawk, D., & N. Gelman. MRI Relaxation Rates in Tumor Cells Expressing MagA Reporter Gene. *London Health Research Day,* London, Ontario, Canada, March 20, 2012.
5. **Sengupta, A**., Rohani, R., Thompson, R.T., Prato, F.S., Goldhawk, D., & N. Gelman. MRI Relaxation rates in Tumor Cells Expressing the MagA Reporter

Gene. *ISMRM ScientificWorkshop* Miami Beach, Florida, USA, January, 2012.

ORAL:

1. **Sengupta, A**., Rohani, R., Thompson, R.T., Prato, F.S., Goldhawk, D., & N. Gelman. MRI Relaxation Rates in Tumor Cells Expressing MagA Reporter Gene. *ImNO, 10th Imaging Symposium* Toronto, Ontario, Canada, February 13-14, 2012.

PROFESSIONAL ASSOCIATION

12/11 – Present	International Society for Magnetic Resonance in Medicine (ISMRM)
13/02 – Present	World Molecular Imaging Society (WMIS)

TECHNICAL SKILLS

Computer:　MS Office, Matlab, C++
Laboratory:　Cell Culture Techniques

CERTIFICATION

1.　Basic Animal Care and Use Course (including sterile injections techniques and basic handling, mouse injections and techniques, mouse anesthesia and assessment monitoring and intervention)
2.　Biosafety training
3.　Workplace Hazardous Materials Information System (WHMIS) for laboratory workers.

LANGUAGES

English, Bengali and Hindi – fluent in speaking, reading and writing